nature portfolio

https://doi.org/10.1038/s41586-026-10867-z

Supplementary information

Upcycling of polyvinyl chloride into polyalphaolefin lubricants

In the format provided by the authors and unedited

Supplementary Materials
for

Upcycling of Polyvinyl Chloride into Polyalphaolefin Lubricants

Eric Munyaneza Nuwayo,[1‡] Connor Thompson,[1‡] Abby Civiello,[1‡] Adrian DiMarco,[2] Jingtao Zhang,[3] Seungjoo Lee,[4] Gugyeong Sung,[4] Tridip Das,[5] Yue Zhang,[1] Clark Vu,[6] Shelby Koshak,[7] John B. Matson,[1,6] Ali Erdemir,[4]* William A. Goddard III,[5]* Xi Chen,[3]* and Guoliang Liu[1,2,6,7,8]*

[1] Department of Chemistry, Virginia Tech, Blacksburg, VA 24061, USA

[2] Department of Chemical Engineering, Virginia Tech, Blacksburg, VA 24061, USA

[3] Department of Industrial and Systems Engineering, Virginia Tech, Blacksburg, VA 24061, USA

[4] Department of Mechanical Engineering, Texas A&M University, College Station, TX 77843, USA

[5] Materials and Process Simulation Center, California Institute of Technology, Pasadena, CA 91125, USA

[6] Department of Materials Science and Engineering, Virginia Tech, Blacksburg, VA 24061, USA

[7] Macromolecules Innovation Institute, Virginia Tech, Blacksburg, VA 24061, USA

[8] Division of Nanoscience, Academy of Integrated Science, Virginia Tech, Blacksburg, VA 24061, USA

[‡] These authors contributed equally to this work

*Corresponding authors. gliu1@vt.edu, xchen6@vt.edu, aerdemir@tamu.edu, wag@caltech.edu.

Contents

1. An extended literature survey of past PVC upcycling strategies

Upcycling is a promising means to enhance the circularity of PVC plastics. Several substitution and C-C bond formation strategies, including Barbier coupling, have been developed to convert PVC into chemically modified polymers with new functionality[1-3]. The difficulty of these strategies lies in achieving quantitative conversions[4]. Alternatively, the comparatively reactive C-Cl bonds in PVC provide an opportunity to "graft from" the C-C backbone through atom transfer radical polymerization and cationic polymerization, creating copolymers of diverse structures[5,6]. In addition, PVC may contain a small amount of tertiary C-Cl bonds[5,7,8], which can be easily activated for functionalization. Partial dehydrochlorination produces allylic C-Cl bonds that are more reactive than secondary C-Cl bonds for dechlorination and functionalization. However, it is a challenge to completely activate all the C-Cl bonds, which limits the grafting density and prevents complete dechlorination[5]. Therefore, the resulting polymers still retain C-Cl bonds; precariously, these polymers can release Cl-compounds during use, raising safety concerns[9].

Similarly, chlorohydrocarbons are undesirable in lubricants due to their environmental hazards and corrosiveness. Thus, upcycling PVC to Cl-free lubricants presents a significant technical challenge. To remove Cl in the upcycled products, a common strategy is to use metal oxides and base Cl scavengers, which generate unreactive metal chlorides[10,11]. This strategy has recently shown success in protecting hydrogenolysis catalysts from deactivation, enabling the co-upcycling of polyolefins with up to 10% PVC into lubricants[12]. However, the sacrificial scavenger agents can impose prohibitive costs in scaled-up operations. In short, existing PVC upcycling strategies thus far have been limited in practicality and hindered by the requirement of expensive and structurally complex initiators, stoichiometric metal hydride sources, and hygroscopic ionic liquids.

2. Controlling the branching and rheological properties of vPAO

Prior computational and experimental studies have shown a strong correlation between lubricant molecular structure and viscosity, as well as viscosity index (VI)[13,14]. Thus, it is imperative to control the molecular structure of lubricants through modulating branching, isomerization, and chain scission during PVC upcycling. Generally, molar mass (M_n) and branching ratio (BR) are two main parameters that significantly influence the viscosity of lubricants. High molar mass and branching are associated with improved viscosity; however, excessive branching worsens the viscosity index[15]. In our process, we control the molar mass and branching by reaction conditions, including $AlCl_3$ loading, temperature, and time. An increasing $AlCl_3$ loading led to a decrease in lubricant molar mass but an increase in branching, resulting in a reduced dynamic viscosity (**Fig. S11**). Thus, 50 mol% of $AlCl_3$ loading with respect to Cl atoms was required to ensure complete dechlorination. Similarly, in the control reactions of alpha-olefin oligomerization without PVC, the effect of catalyst loading on the M_n and branching was also observed. Reducing the $AlCl_3$ loading resulted in lubricants with fewer branching sites, as evidenced by the high CH_2/CH_3 integral ratios, which are in line with typical cPAO (**Fig. S9c)**. Conversely, the yield increased slightly, and the viscosity increased, likely due to less chain fragmentation (**Figs. S9b, S9d,** and **S9e**). Additional factors demonstrated a substantial effect on branching in the PVC upcycling reaction, namely, solvent type and α-olefin chain length (**Schemes S1**, **S3**, and **S4**). We should clarify that in the current process, branching can result from α-olefin oligomerization at the side chains (i.e., the chains linked to the PVC backbone), as well as chain cleavage and isomerization under highly Lewis acidic conditions.

The use of aromatic solvents, such as toluene, suppressed the α-olefin oligomerization at the side chain through Friedel-Crafts alkylation, which, in turn, minimized the degree of branching, as evidenced by the CH_2/CH_3 integral ratio from ^1H NMR (1.8 in toluene compared to 0.9 in DCM) (**Fig. S16** and **Table S4**). Similarly, non-chlorinated hydrocarbon solvents (e.g., hexanes) led to minimal branching in real-world PVC-derived lubricants (**Table S4**). To confirm that hexanes minimize branching caused by chain walking and isomerization, we evaluated spectroscopic data from DEPT NMR and HSQC of two waste-derived lubricants, focusing on the β-CH_2 and isopropyl-type CH_3 signals at 22.6 - 22.9 ppm in ^{13}C spectra. The DEPT 135 NMR of PVC waste-based v_{10}PAO synthesized in DCM featured overlapping CH_3 and CH_2 peaks at 22.6 - 22.9 ppm, which showed a correlation with both methylene and methyl ^1H NMR signals in HSQC (**Figs. S22** and **S32**). Conversely, v_{10}PAO synthesized in hexanes displayed mainly a negative CH_2 peak at 22.7 ppm in DEPT 135 with a strong HSQC cross peak at {1.3, 22.7} ppm and a weak CH_3 cross peak at {0.9, 22.7} ppm compared to v_{10}PAO-mix-DCM (**Figs. S22** and **S32**). The weak intensity of the methyl group cross-peak stems from suppressed isomerization pathways through hydrogen transfer from the solvent. Therefore, hexanes promoted relatively low levels of branching as indicated by minimal isopropyl groups in the upcycled oils. Lastly, ^1H NMR and ^{13}C NMR analyses revealed the least branching and isomerization in lubricants synthesized using long-chain α-olefins, as indicated by dynamic viscosity measurements. Lightly branched lubricant v_{10}PAO, synthesized from PVC and 1-decene, showed the lowest viscosity, in contrast to their highly branched counterparts synthesized from shorter-chain α-olefins (**Fig. S3**)[16,17]. Overall, to synthesize vPAO with a good viscosity index and tribological performance, it is crucial to minimize branching by judiciously selecting the α-olefin, the solvent, and the catalyst loading.

3. Comparison of lubricant properties of α-olefin reactions with and without PVC

The introduction of PVC into the upcycling reactions leads to PAO with different molecular structures than those without PVC (**Fig. S10a**)[18]. Foremost, the PVC backbone template provides a platform for alkylation reactions with α-olefins, which afford vPAO with a relatively high molar mass of ~1270 g/mol, compared to ~870 g/mol for cPAO (**Fig. S10c**). In addition, side reactions may involve unsaturated and saturated chlorocarbons formed during PVC degradation, producing lubricants with different levels of branching (**Scheme S4**). Both molar mass and degree of branching greatly influence lubricant properties, including viscosity and thermal properties[19,20]. For instance, vPAO showed over thirty times increase in dynamic viscosity and about five times increase in kinematic viscosity at 40 °C compared to cPAO (**Figs. S10d** and **S10e**). vPAO also exhibited a T_g of -54°C (vs. -62 °C for cPAO) due to restricted segmental mobility (**Fig. S10f**)[21]. The effect of branching was further illustrated in tribology studies where PVC-derived vPAO synthesized in DCM led to a deep scar with a wear volume of 243,000 μm^3, in contrast to cPAO with about ten times less wear volume (24,900 μm^3, **Figs. S10g and S10h**). The relatively poor tribological performance is attributed to short-chain branching, as introduced via PVC degradation moieties in DCM solvent, which hinders the formation of a robust film at the interface during testing[22,23]. These results reveal clear structural differences in cPAO and vPAO, and the vastly distinct material properties reinforce that PVC skeletal moieties are incorporated into the final molecular structures.

The branching ratio (BR) of the lubricants was calculated according to the following equation,

$$BR = \frac{15 \int_{10.8\ ppm}^{22.7\ ppm} C13\ \ signal}{15 \int_{10.8\ ppm}^{22.7\ ppm} C13\ signal + 14 \int_{22.7\ ppm}^{44\ ppm} C13\ signal} \times 100\%$$

Generally, methine (CH) peaks are omitted in the integration due to their low intensities[24,25]. To ensure that the branching ratio values accurately reflect the mass ratio of CH_2/CH_3, we collected DEPT-315 spectra of v_6PAO, v_8PAO, and v_{10}PAO synthesized from lab-grade PVC, in addition to mixed-waste-based v_{10}PAO synthesized in DCM and hexanes to exclude methine signals from the integration.

4. Quantification of the gas phase and structure identification with GC-MS analysis

We estimated the gas fractions in the reactions based on mass conservation in a closed system. Without α-olefins, the control reaction generated the most volatile products, due to unabetted dehydrochlorination to HCl and short-chain hydrocarbons (**Figs. S4 and S33a**). With α-olefins, the upcycling reaction in CH_2Cl_2 produced fewer gaseous products because the alkylation reaction between dechlorinated PVC and α-olefins attenuated backbone chain scissions. Furthermore, via hydrogen transfer to carbenium, the upcycling reaction in hexanes effectively reduced the extent of chain scission to produce short-chain hydrocarbons (**Scheme S3**), resulting in the least gas products. In addition, size-exclusion chromatography (SEC) revealed a higher molar mass of vPAO prepared in hexanes than in CH_2Cl_2 (1660 kDa vs. 1270 kDa, respectively), further confirming that hydrogen transfer to the carbenium obstructed PVC chain cleavage (**Fig. S33b**).

To perform qualitative analysis of gaseous products, the contents of the Schlenk tube headspace were passed over ZnO to neutralize HCl before injection into GC-MS. All reactions with α-olefins featured isoalkanes, mostly saturated and minor naphthene products. Naphthene-type structures were formed through intramolecular cyclization of carbocations and unsaturated sites. However, this pathway was minor owing to intermolecular alkylation of the PVC backbone with α-olefins and hydrogen transfer from the solvent. Hydrocarbon gases were not detected in the control reaction without α-olefins (**Fig. S7**). The absence of hydrocarbons in the GC-MS of the control reaction suggests that extensive dehydrochlorination generated mostly gaseous HCl. However, isoalkanes and unsaturated products, along with minor chloroalkanes, were detected in the solution from the control reaction. (**Figs. S4d and S4e**).

5. Quantification of trace residual chlorine in lubricants

To determine ppm-level chlorine content in upcycled lubricants, we performed ion chromatography on lab-grade PVC-derived v_8PAO and mixed-waste PVC-derived v_{10}PAO prepared in DCM and hexanes. The lubricants were first subjected to Schöniger oxidation to mineralize organic chlorine, and the products were dissolved in a hydrogen peroxide solution for further analysis. All lubricants contained < 100 ppm chlorine, and v_{10}PAO mix hexanes showed the lowest levels of chlorine based on the area under the curve in the chromatogram (**Fig. S12** and **Table S3**). The oils prepared in DCM (v_8PAO and v_{10}PAO-mix-DCM) contained slightly higher chlorine, likely due to possible side reactions involving the solvent and the Lewis acid (**Schemes S2** and **S4**). Therefore, the dechlorination and alkylation of PVC drastically decrease the concentration of chlorine to < 100 ppm in the lubricant, representing > 99.98% chlorine reduction.

6. $AlCl_3$ dechlorination efficiency in hexanes under dry and humid conditions

Previous work has established that chloromethanes can react with $AlCl_3$ to produce chloromethyl cations, diverting $AlCl_3$ from the PVC dechlorination reaction[26]. Therefore, we considered alternative solvents such as hexanes. To establish the effect of solvent on $AlCl_3$ loading, PVC was reacted with 1-octene in hexanes using 10-50 mol% $AlCl_3$. At low $AlCl_3$ loadings (< 28 mol%), the lubricants and solid byproducts featured discernible residual chlorine as indicated by peaks associated with C-Cl in both FTIR and ^{1}H NMR (**Fig. S17**). Complete dechlorination was attained at ≥ 28 mol% $AlCl_3$ loading, representing a 1.8-times increase in efficiency compared to the reactions in DCM. Therefore, solvents such as alkanes, despite their lower solubilities for PVC, are effective and suitable for PVC dechlorination and alkylation. Attempts to lower $AlCl_3$ loadings in DCM reactions were unsuccessful, even after extending the duration to 48 h. The product obtained using 25 mol% $AlCl_3$ in DCM contained residual PVC, as indicated by a strong C-Cl peak at 617 cm^{-1} in the FTIR and the set of protons centered at 4.4 ppm, associated with nearby chlorine, in the ^{1}H NMR (**Figs. S34b and S34c)**. The molar mass of the product, which appeared greasy, dropped in comparison to the 20 mol% $AlCl_3$ loading, likely due to a high extent of chain scissions **(Fig. S35**).

To further improve catalyst efficiency, future efforts should focus on developing supported, high-surface-area, deactivation-resistant catalysts that are easily recoverable for large-scale synthesis[27]. It is worth exploring alternative Lewis acids, such as BF_3 and tris(pentafluorophenyl)borane, which are potentially more catalytically active. We did not investigate them due to safety concerns in a laboratory setting.

We further investigated additional factors that could lower the activity of $AlCl_3$. For example, the high oxophilicity of $AlCl_3$ could cause reactions with moisture, reducing the activity of $AlCl_3$[28]. Indeed, adding 2 - 10 wt.% water to $AlCl_3$ in the upcycling of PVC with 1-decene resulted in decreased lubricant yield, leaving behind an increasing amount of residual solid, likely partially dehydrochlorinated PVC (**Fig. S31**). This reduced reactivity can be attributed to the formation of aluminium chlorohydrates, whose Lewis acidity was much weaker than that of $AlCl_3$. To minimize the effect of water in a large-scale process, $AlCl_3$ could be heated before feeding it into the main reactor. To ensure catalyst recyclability, the HCl produced during the reaction (**Fig. S5**) can also be used to convert chlorohydrates back to $AlCl_3$, as indicated in **Scheme S5** and process flow diagram (PFD) (**Fig. S36**).

7. The timing of α-olefin addition

The timing of α-olefin addition influenced the lubricant yield. During an attempted synthesis of v_8PAO, we inadvertently delayed the introduction of 1-octene, resulting in the formation of solid products. Therefore, we systematically investigated the effect of delaying the addition of 1-octene. When the addition of 1-octene was delayed up to 5 min, the reaction did not generate any significant amount of solids (**Fig. S29b**). However, when 1-octene was added after a 10-min delay at 0 °C, it resulted in 184 mg of solid product. Further delays of over 10 min increased the amount of the solid product.

Structural analysis revealed that the solid products consisted of partially alkylated polyene-like material, similar to the control reaction without α-olefin, differing only in the degree of alkylation (**Fig. S29a**). Presumably, before the addition of α-olefin, HCl was released from PVC and further accelerated the dehydrochlorination of PVC[29], yielding a partially alkylated polyacetylene. Therefore, to prevent the formation of insoluble polyacetylenes and the conversion of PVC to low-

value carbonaceous materials, α-olefins should be added immediately once the solvent is introduced into the reaction. Alternatively, a solution of α-olefins in a selected solvent should be slowly added to a mixture of $AlCl_3$ and PVC. Attempts to add $AlCl_3$ to a stirred mixture of PVC and α-olefin are discouraged due to the violent bubbling that occurs in the reaction vessel.

8. Effect of solution concentration

To explore the effect of solution concentration on the structure and properties of vPAO, we set up two 3-h reactions using 5 ml and 10 ml of DCM. The yield of the lubricant in 5 ml DCM (v_8PAO-5ml) dropped to 51.6% from 64.4% for the lubricant in 10 ml DCM (v_8PAO-10ml) **(Fig. S30a**). Due to its poor solubility, PVC formed a suspension in DCM. The smaller amount of DCM solvent caused relatively inefficient suspension of PVC, and thus, the dechlorination reaction did not proceed to completion. As a result of incomplete dechlorination, minor proton resonance peaks attached to the C-Cl bond were detected at 4.4 ppm (**Fig. S30c**). In addition, $vPAO_8$-5ml displayed a low decomposition temperature at 5% weight loss ($T_{d5\%}$) of 170 °C, possibly due to the early onset of dehydrochlorination. Conversely, the product of dehydrochlorination exhibited high thermal stability and degraded at temperatures exceeding 450 °C (**Fig. S30b**). The presence of partially dechlorinated products was further evidenced by the size exclusion chromatography (SEC) results, which revealed a high molar mass fraction and broad dispersity in the chromatogram that was not exhibited by the product obtained under low-concentration reaction conditions (**Fig. S30d**). As expected, the presence of high M_n fractions in the $vPAO_8$-5ml sample resulted in a viscous oil with about twice the dynamic viscosity of $vPAO_8$-10ml (**Fig. S30e**). Altogether, these results show that concentration is a critical variable in the upcycling reaction, and it can regulate the viscosity and overall performance of lubricants.

9. Characterization of solid byproducts from reactions using alternative Lewis acids

PVC upcycling using anhydrous $FeCl_3$, BF_3OEt_2, and Sb_2O_3 generated white solid by-products. The reaction using $FeCl_3$ catalyst produced 26.7 wt.% of partially dechlorinated and partially alkylated solid. The partial dechlorination and partial alkylation were confirmed by thermogravimetric analysis (TGA), showing a ~ 52 wt.% dehydrochlorination weight loss compared to a ~ 63 wt.% loss in virgin PVC, and FTIR, exhibiting strong C-H stretch bands **(Fig. S15b** and **Fig. 2f**). In addition, the differential scanning calorimetry (DSC) trace of the solid product revealed a slight decrease in the glass transition temperature compared to PVC, presumably due to the plasticizing effect of the attached alkyl chains (**Fig. S15c**). We observed no significant change in molar mass (**Fig. S15d**). The attachment of alkyl chains did not result in any sharp 2θ peaks in the X-ray diffraction (XRD) spectrum, and the diffraction pattern resembled that of PVC, indicating no measurable change in crystallinity at low levels of alkylation (**Fig. S37**). Accordingly, there was no noticeable melting endotherm in the DSC (**Fig. S15c**).

The solid product could be swollen in $CHCl_3$ at room temperature to produce a gel-like material, and the solubility improved at higher temperatures. The improved solubility enabled us to record ^{1}H NMR spectra in $CDCl_3$, which exhibited alkyl chain proton peaks between 0.7 and 1.5 ppm and hydrogen near C-Cl at 2.2 - 4.4 ppm (**Fig. S38**). The solid product also exhibited good solubility in hot trichlorobenzene, similar to low-density polyethylene (LDPE) (**Fig. S39)**[30]**.** Therefore, we plan to investigate the performance of alkylated PVC products further in the future.

In reactions catalyzed by BF_3OEt_2 and Sb_2O_3, the solid products exhibited structural characteristics, thermal properties, and solubility similar to virgin PVC, indicating that these Lewis

acids are ineffective for PVC dechlorination under our experimental conditions (**Figs. S15b** and **S15c**).

10. Effects of additives on PVC upcycling

PVC pipes, toy frogs, and cards were dissolved in THF and precipitated in water to obtain PVC powders. Without undergoing further purification to remove organic additives, the dried PVC powders were upcycled using 1-octene in DCM with $AlCl_3$.

Due to the potential presence of organic additives, the reaction yielded lubricants in low to moderate yield. The products appeared dark brown even after hydrogenation utilizing a 15 wt.% Pd/C catalyst (**Figs. S40a** and **S40b**). Structural analysis of the lubricant revealed additional peaks in the ^{1}H NMR and FTIR spectra, in addition to the typical CH, CH_2, and CH_3 signals found in vPAOs synthesized from pure PVC (**Figs. S40c** and **S40d**). For example, FTIR spectra displayed ester C=O and aromatic C=C signals, likely originating from common PVC additives and plasticizers (e.g., phthalates), which were absent in the spectra of vPAO from cleaned PVC waste (**Fig. S41**). As shown by ^{1}H NMR, aromatic peaks appeared in these lubricants.

Due to detrimental interactions between additives and $AlCl_3$ (i.e., reduced activity of the Lewis acid), the reactions generated solid residues consisting of unreacted PVC and other by-products, amounting to ~ 3.2 - 15.3 wt.% of the initial mass of the feedstocks (**Fig. S40a**).

To avoid the unfavorable interactions caused by additives and to synthesize high-quality lubricants, we dissolved the PVC waste in THF and filtered off the insoluble residues. The THF solution was then precipitated in water to remove water-soluble salts. The precipitate was redissolved in THF and precipitated in isopropanol to remove organic additives (e.g., phthalate plasticizers). ICP-MS was used to analyze the purity of PVC powder extracted from waste. Unpurified waste powders contained substantial amounts of Ca, Mg, Zn, Ti, and Al due to additives used in PVC products (**Table S5**). Ti is typically associated with UV protection, and Al is linked with flame retardancy[31-34]. In contrast, the purified PVC powders showed reduced concentrations of Ti (down to 101 ppm) and Al (down to 0 ppm). However, considerable amounts of Ca (2,232 ppm) were still detected in the purified powders, but their further removal can be accomplished by using dilute HCl during purification. Notably, < 10 ppm of Ti was found in the final vPAO, likely due to additional filtration steps after synthesis (e.g., passing through activated carbon of Pd/C catalyst). Despite some residual impurities (**Fig. S20**), the upcycling reactions of PVC with 1-octene yielded v_8PAO, and the alkylation was confirmed by the strong alkyl CH_2 and CH_3 signals at 0.6-1.8 ppm in ^{1}H NMR (**Fig. S21**). Similar to lab-grade PVC, the upcycling reaction led to a drastic reduction in the molar mass of the products to M_n < 2,000 g/mol, confirming extensive chain scission of waste-derived PVC under our reaction conditions (**Fig. S23a**). The lubricants unveiled glass transition temperatures (T_g) in the range of -54 °C to -50 °C (**Fig. S23b**) and good thermal stability with a $T_{d5\%}$ of >185 °C and > 57 wt.% after the ASTM D5800 test (**Figs. S23d** and **S23e**), signifying potential applications across a wide range of temperatures (**Fig. S24a)**.

The lubricant yield was determined according to **Equations (S5.1)** and (**S5.2)**, where $m_{product}$ denotes the mass of product after workup, $m_{\alpha\text{-}olefin}$ is the mass of olefin used per reaction, and m_{PVC} denotes the mass of PVC used for the reaction. The constant 0.433 represents the fraction of carbon and hydrogen content in the PVC.

$$Total\ Yield(wt\%) = \frac{m_{product}}{m_{\alpha-olefin} + m_{PVC}} \times 100\% \quad \textbf{(S5.1)}$$

$$Carbon\ and\ Hydrogen\ Yield(wt\%) = \frac{m_{product}}{m_{\alpha-olefin} + 0.433m_{PVC}} \times 100\% \quad \textbf{(S5.2)}$$

11. Long-term stability of waste-derived lubricants

To determine whether residual trace chlorine affects the long-term stability of the lubricants, we evaluated the coefficient of friction and wear volume of a six-month-old v_{10}PAO-mix-hexanes lubricant. Wear tests revealed a wear loss volume (WLV) of ~1400 μm^3, which was lower than that of PAO10 and PAO40 (**Figs. 4c** and **S42**). Although the 3D non-contact profilometer suggested an increase in WLV from 619 μm^3, the 2D line-scans over the wear scars showed almost no differences in the spherical contour of the wear scars (**Fig. S42**). Overall, the wear remained minimal with the steel ball showing no signs of wear, exhibiting only slight abrasive marks. The coefficient of friction remained almost unchanged (~ 0.08), suggesting tribological stability over an extended period of time. Therefore, it is reasonable to conclude that the trace chlorine in vPAO did not drastically compromise the long-term rheological and tribological performance.

12. Techno-economic analysis

12.1 Process design at an industrial Scale for techno-economic analysis

The techno-economic analysis (TEA) was conducted at an industrial scale of 50,000 tons per year, with a batch capacity of 2,080 kg.

12.1.1 Process design

1. A Sankey diagram illustrating the major process streams and products is presented in **Fig. 4d**, while a simplified process flow diagram (PFD) is shown in **Fig. S36**. The process design is based on the following configuration: Production capacity: 50,000 tons of vPAO lubricant per year; batch reaction scale: 2,080 kg; operation time per batch: 4.8 hours.
2. Reaction conditions: heating at 70 °C, and a reaction vessel pressure of 3 bar.
3. Mass feed ratio: PVC/1-decene/$AlCl_3$ = 2/5/3.
4. Hexane loss percentage: 10%.
5. Catalyst recycling: 90% of Raney nickel recovered for reuse.

The process is divided into two primary stages. In the first stage, PVC, 1-decene, and $AlCl_3$ are fed into Reactor 1 under mild thermal conditions, with hexanes serving as the solvent. The reaction yields vPAO and allows for high solvent recovery through downstream distillation, although a small portion of hexanes is lost due to evaporation and participation in the reaction. A water quench step facilitates the recovery of approximately 60% of $AlCl_3$ for reuse. The resulting vPAO stream is then transferred to Reactor 2 for hydrogenation, where it reacts with hydrogen gas in the presence of Raney Nickel. Upon reaction completion, Raney Nickel is separated and recovered for future use. The final product, saturated vPAO, is then collected and stored. By integrating closed-loop recovery systems for both the solvent and catalyst, the process improves overall sustainability and enhances economic efficiency.

12.1.2 Key equipment designs

The primary equipment and accessories—including two reactors, a distiller, two heat exchangers, and two vacuum pumps—are designed for batch processing at a scale of 2080 kg per batch. To meet the annual production target of 50,000 tons, 16 batches are operated in parallel. These components form the basis for equipment cost estimation and the subsequent TEA. Detailed specifications of the equipment design are provided below.

Reactor Design: First stage
The reactor used in the first stage should be constructed with a glass liner and capable of operating at pressures between 3 and 5 bar. For a batch capacity of 2080 kg, the first-stage reaction requires the following inputs: 854 kg of PVC, 1,095 kg of $AlCl_3$, 5,130 L of hexanes, and 2,010 kg of 1-decene. Under the specified reaction conditions of 70 °C and 3 bar, the total required reaction volume is estimated to be approximately 15,000 liters.

Reactor Design: Second stage
The reactor used in the second stage does not require any specific material constraints. For a batch capacity of 2,080 kg, the second-stage reaction requires approximately 120 kg of Raney Nickel, a widely available and easily recyclable catalyst used as an alternative to Pd/C. The estimated reaction volume for this stage is approximately 3,500 liters.

Distillation design
A batch distillation setup using a still pot is employed to separate vPAO from hexane. The entire reaction mixture is charged into the still pot, which is then heated. Due to its higher volatility relative to vPAO, hexane vaporizes first and is removed from the system, leaving behind the purified vPAO.

The total batch volume determines the size of the still pot. The feed consists of 2080 kg of vPAO and 5,130 L of hexane, for a total liquid volume of 7,670 L. To prevent entrainment or carry-over of boiling liquid into the vapor outlet, the still pot must include sufficient headspace. Therefore, a still pot with a total volume of at least 10,000 liters is used to ensure safe and efficient operation.

12.2 Considerations of converting PVC waste to PAO lubricant

12.2.1 Assumptions for conducting TEA at an industrial scale

Key capital investment assumptions are presented in **Table S7**. Additional critical assumptions for the base case are detailed in **Tables S8** and **S9**, including project duration, salvage value, depreciation method and period, annual interest rate, fixed costs (such as raw material and product prices), operating labor, supervision, utilities, maintenance and repairs, operating supplies, laboratory expenses, royalties, plant overhead, and general expenses. In a 2-ton reactor, the 1-decene loading can be reduced by optimizing the α-olefin feed rate, an adjustment that is less consequential for small-scale reactions but can help minimize undesired oligomerization reactions. Moreover, it is reasonable to assume that all 1-decene in the feed reacts under highly cationic conditions, eliminating the need for additional costs associated with distilling unreacted olefins. In the TEA, the plant is modeled with an annual production capacity of 50,000 tons, corresponding to 2,080 kg per batch.

12.2.2 Chemical price analysis

Key material prices were determined through market investigations and reputable data sources. The price of PAO lubricant was obtained from a Q4 2024 market survey[35], while hydrogen pricing was sourced from a 2030 forecast published by Statista®[36]. PVC waste pricing was derived from a Q2 2025 market investigation. The cost of 1-decene was drawn from a U.S. market study conducted in June 2023[37]. The price for $AlCl_3$ catalyst was sourced from market surveys in China in December 2023[38]. Nitrogen and hexane prices were derived from Q1 2025 market analysis[39,40], and the cost of Raney Nickel was drawn from a European market investigation conducted in December 2023[41].

12.2.3 Capital investment

Based on the process design, we estimated fixed and total capital investments using the Percentage of Delivered-Equipment Cost method[42]. Equipment sizes were determined to establish a preliminary industrial process, and their costs were estimated using market price research combined with the six-tenths-factor rule. The resulting cost estimates for a single batch are presented in **Table S9**, and total equipment costs were calculated by multiplying these values by 16. Additional components, such as direct costs, were computed as percentages of the purchased equipment cost. Further elements of capital investment were derived using average percentages of the total direct cost and the combined total of direct and indirect costs.

12.2.4 Product cost and revenue

Total product costs include both manufacturing and general expenses. Manufacturing costs encompass all expenditures directly related to the production process or related equipment. The estimation began with raw material costs, followed by other direct production costs, which were calculated as percentages of either the total product cost or labor costs. Raw material costs were determined based on the chemical inputs and prices listed in **Table S8**. To produce 100 kg of lubricant, the process requires 115 kg of 1-decene, 49.3 kg of PVC, 52.6 kg of aluminum chloride, 246 L of hexanes, 5.77 kg of Raney Nickel, 1.58 kg of nitrogen, and 0.0780 kg of hydrogen.

Fixed charges include depreciation, local taxes, insurance, rent, and financing interest. These costs are generally influenced by fixed capital investment and typically account for 10% to 20% of the total product cost. Plant overhead costs typically cover general plant maintenance, payroll overhead, packaging, medical services, safety and protection, dining facilities, recreation, salvage, laboratories, and storage, usually accounting for 5% to 15% of the total product cost. General expenses encompass administrative costs, distribution and selling expenses, and research and development, typically ranging from 9% to 37% of the total product cost[43].

Gross earnings are determined by subtracting the total product cost from total revenue. Revenue is generated from the sale of products produced by the plant. The total annual revenue from product sales is calculated by summing up the products of each item's unit price and its sales rate.

12.2.5 Profitability

Profitability is evaluated using four key metrics: return on investment (ROI), payback period (PBP), net present value (NPV), and internal rate of return (IRR). While ROI and PBP provide straightforward assessments, they do not consider the time value of money. In contrast, NPV and

IRR incorporate the time value of money, offering a more comprehensive financial analysis. The calculation methods for each metric are outlined below.

Return on Investment (ROI) is calculated as the ratio of net profit to total investment, as shown in **Equation (S5.3)**:

$$\text{ROI} = \frac{\text{annual net profit}}{\text{total capital investment}} . \quad \textbf{(S5.3)}$$

Payback period (PBP) refers to the number of years required for the cumulative returns to equal the initial fixed capital investment. It can be calculated using **Equation (S5.4)**:

$$\text{PBP} = \frac{\text{fixed capital investment}}{\text{average annual net cash flow}} . \quad \textbf{(S5.4)}$$

The annual net cash flow generated by the entire project and returned to the capital reservoir is determined using **Equation (S5.5)**:

$$A_j = \left(s_j - c_{oj}\right)(1 - \Phi) + d_j\Phi , \quad \textbf{(S5.5)}$$

where A_j represents the cash flow from the project to the corporate capital reservoir in year j, s_j is the sales revenue in year j, c_{oj} denotes the operating costs (excluding depreciation) in year j, d_j is the depreciation expense in year j, and Φ is the fractional income tax rate. **Depreciation** is calculated using the straight-line method, which assumes the asset's value decreases uniformly over its recovery period, with a salvage value of zero. The annual depreciation is determined using **Equation (S5.6)**:

$$\text{Annual depreciation} = \frac{\text{OPI}}{\text{LRP}} . \quad \textbf{(S5.6)}$$

where OPI refers to the initial property investment at the start of the recovery period, and LRP denotes the length of the straight-line recovery period.

Net present value (NPV) is calculated as the difference between the present value of all future cash flows and the present value of the total capital investment (TCI), as shown in **Equation (S5.7)**:

$$\text{NPV} = \sum_{j=1}^{n} \frac{A_j}{(1+r)^j} - \text{TCI} \quad \textbf{(S5.7)}$$

where A_j denotes the nominal net cash flow in year j, r is the discount rate, and n is the project lifetime (in years).

The internal rate of return (IRR) is the discount rate that sets a project's NRV to zero. It represents the break-even rate of return, where the present value of future cash flows equals the initial investment. The IRR is determined by solving for the discount rate *r* that sets the NPV in **Equation (S5.7)** equal to zero.

12.2.6 Results of TEA at an industrial scale

The TEA is based on a production capacity of 50,000 tons per year of PAO lubricant. In the base-case scenario, the fixed capital cost is estimated at $72.89 million, with 21.1% allocated to purchased equipment, 65.9% to other direct costs, 21.1% to indirect costs, and 8.1% to other costs.

The total capital investment (TCI) amounts to approximately $83.83 million, including $10.93 million in working capital.

Assuming full production capacity, the annual sales revenue is estimated at $160.6 million, with annual product costs (excluding depreciation) of $7.29 million. This results in a gross profit of $24.23 million and a net profit of $19.66 million. Based on these figures, the project achieves an IRR of 22.80%, a PBP of 4.26 years, and an average ROI of 23.45%.

Sensitivity analysis. A sensitivity analysis was conducted to evaluate how variations in key design and cost assumptions affect project profitability. **Fig. 4f** shows a tornado diagram illustrating the impact of key economic variables on the IRR of the project. Among the factors analyzed, the PAO price exerts the most significant influence on IRR: a 10% increase raises IRR by approximately 15%, while a 10% decrease lowers it by approximately 16%, highlighting its high sensitivity. The price of 1-decene also significantly affects IRR, with ±7% price changes resulting in approximately ±10% IRR deviations. In contrast, equipment costs have a moderate effect (±2–3%), and the PVC price has minimal impact, with IRR remaining nearly unchanged under ±10% variations. Overall, these results indicate that PAO and 1-decene prices are the primary drivers of project profitability, whereas capital expenditures and other material costs play a comparatively minor role. The overall profitability of the project demonstrates low sensitivity to the prices of other raw materials (**Fig. S27)**. Inputs such as PVC, $AlCl_3$, nitrogen, and hydrogen exhibit minimal influence on IRR across a ±30% price variation, with the corresponding IRR curves remaining relatively flat. These results suggest that the project is resilient to fluctuations in the prices of most raw materials, highlighting the robustness of the economic model under varying market conditions. **Fig. S28** illustrates the effect of equipment cost changes on the project's payback period, showing a clear positive correlation: higher equipment costs lead to longer payback periods. Specifically, a 30% reduction in equipment cost shortens the payback period to approximately 2.4 years, whereas a 30% increase in equipment cost extends it to over 6 years. Despite these variations, the project remains economically viable across the full range of equipment cost changes examined.

13. Additional schemes, figures, and tables

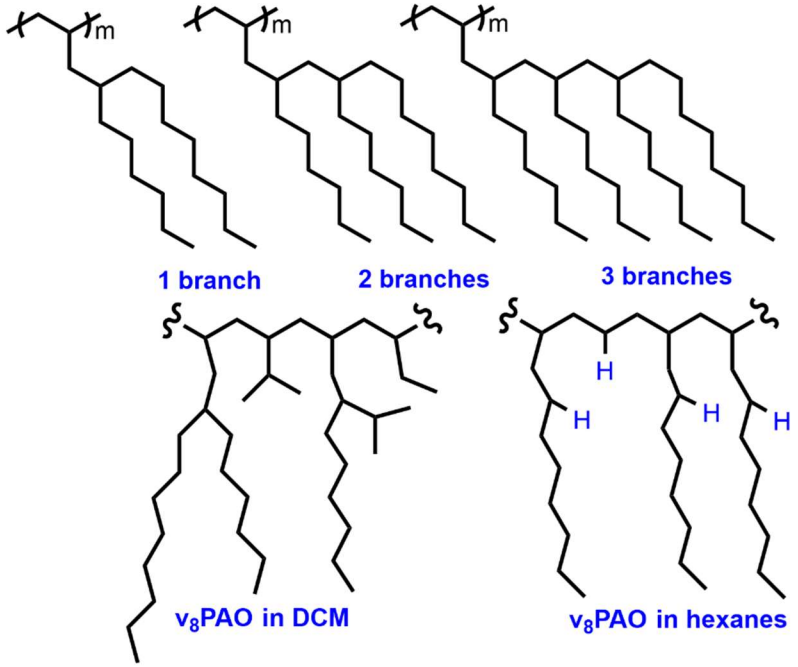

Scheme S1. Schematic illustration of **(Top)** PVC-initiated α-olefin oligomerization at one activated site to form "branch-like" structures and **(bottom)** α-olefin substitution at multiple activated sites. The solvent plays a role in the PAO chemical structure during the PVC-templated substitution of Cl with α-olefins. Compared to DCM, hexanes quench α-olefin oligomerization and minimizes short-branch formation, thus reducing the overall branching in PAO to form "comb-like" structures.

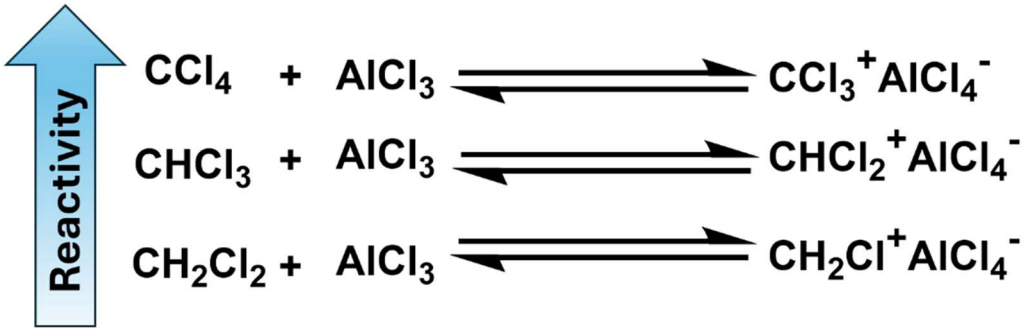

Scheme S2. Reactivity of chloromethanes with Lewis acids. The reactivity increases with increasing chlorination of chloromethanes[44].

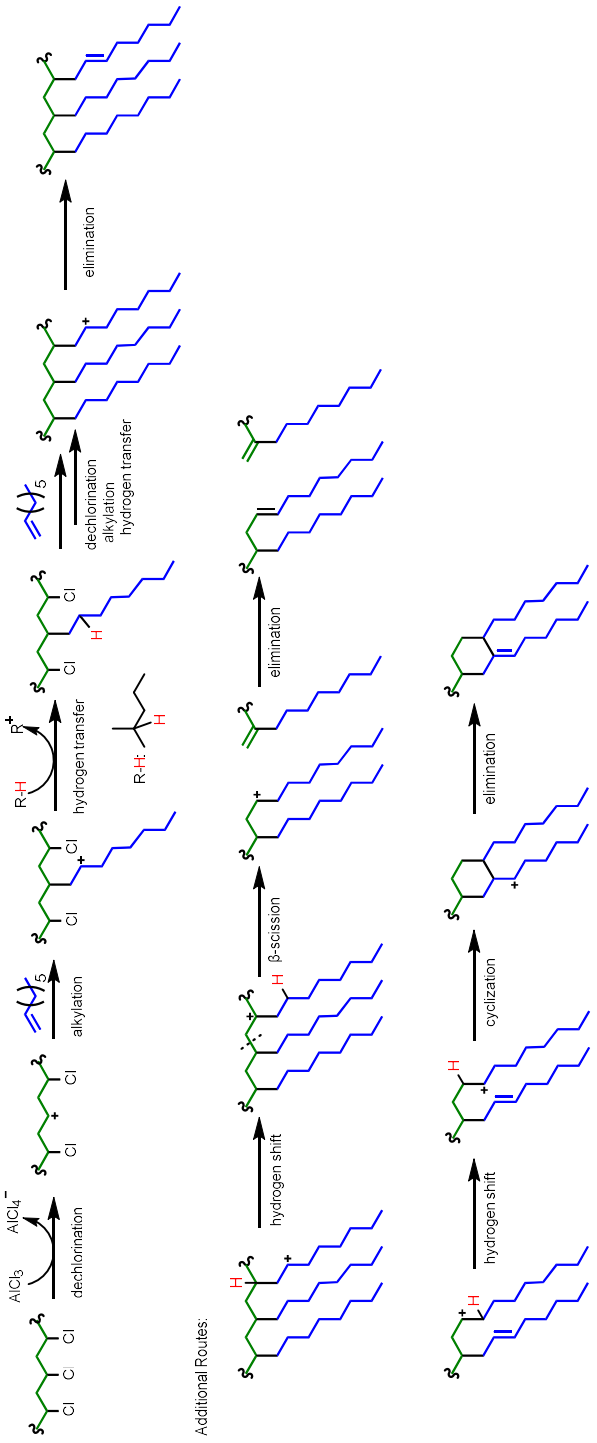

Scheme S3. Proposed mechanism of PVC upcycling in hexanes. Carbocations shift or are quenched via either intramolecular hydrogen shift or intermolecular hydrogen transfer with solvent. Note: The H-transfer and elimination reactions do not necessarily proceed in sequence, and the scheme is to illustrate the possible reaction pathways such as alkylation, β-scission, and cyclization.

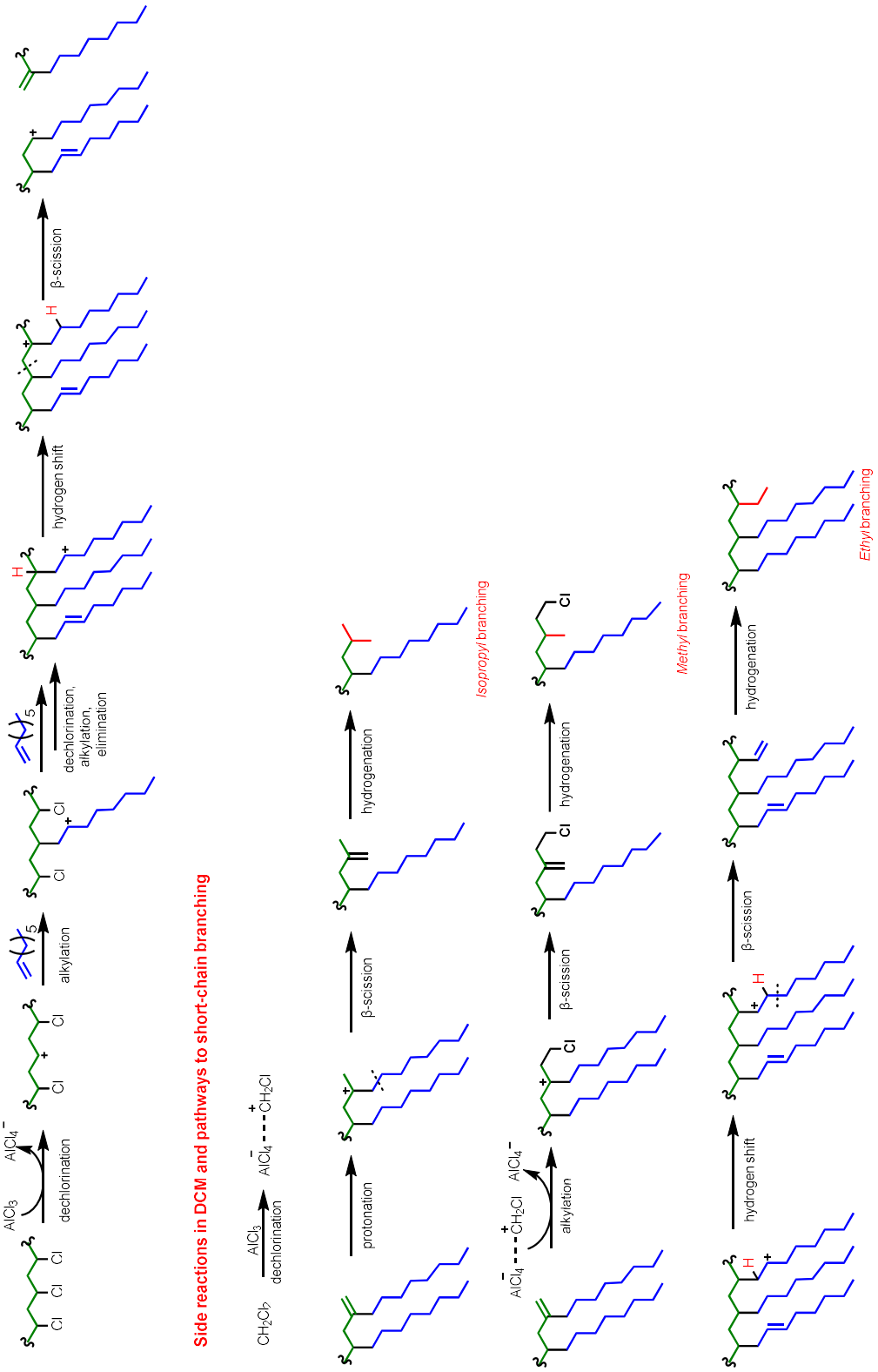

Scheme S4. Upcycling of PVC in DCM. The solvent can participate in the dechlorination and alkylation pathways, leading to residual chlorine in vPAO and increased branching.

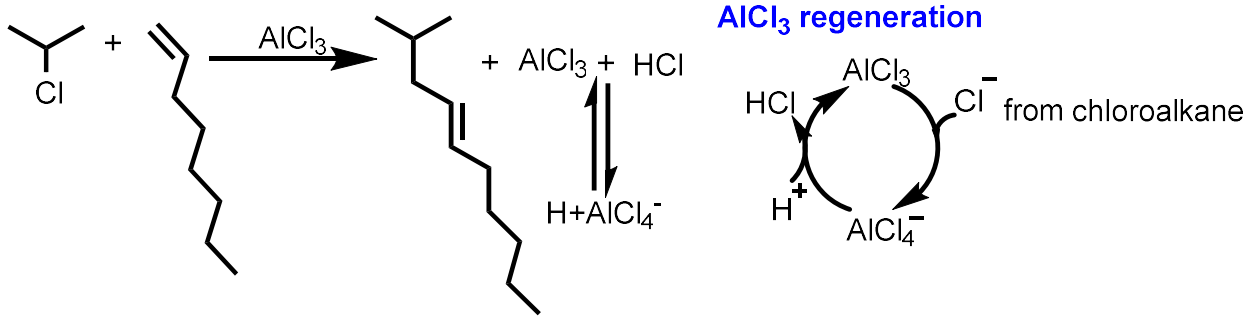

Scheme S5. **Dechlorination-alkylation reaction of a model chloroalkane substrate**. In principle, $AlCl_3$ can turn over after dechlorination if free protons are present in the reaction solution.

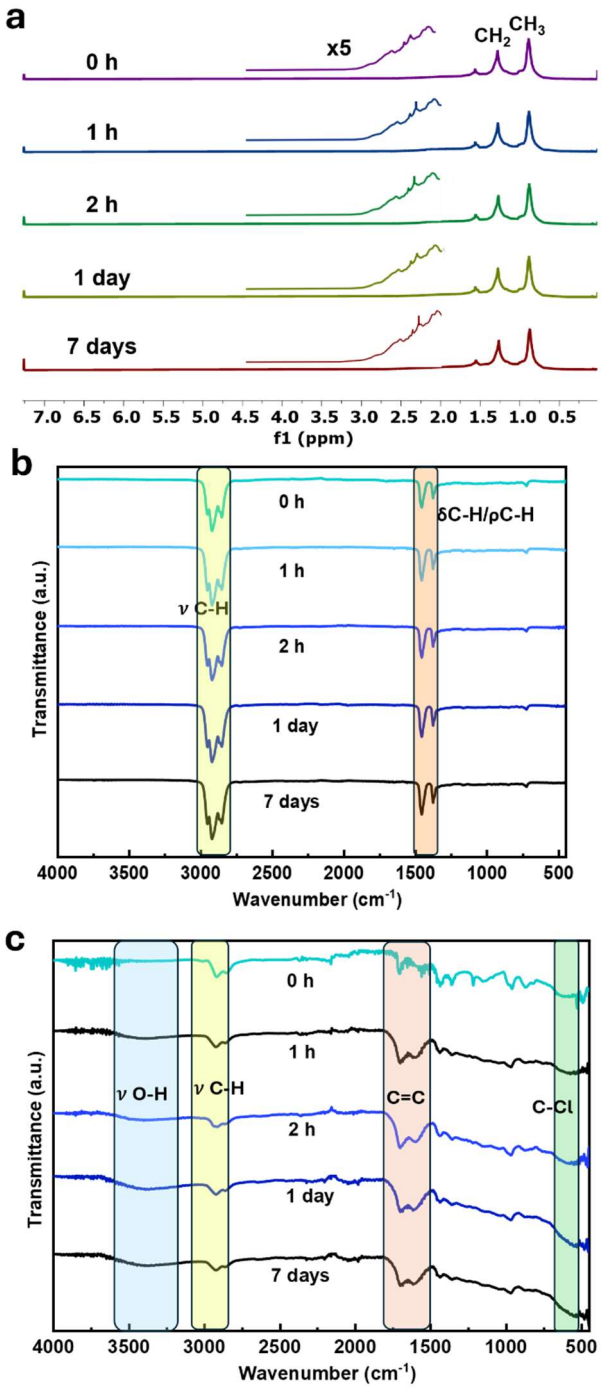

Figure S1. Comparative study on the oxidation stability of polyene versus v$_8$PAO. a) Time-resolved ^{1}H NMR spectra of v$_8$PAO left on a bench for 7 days. No noticeable changes were observed between 1.9 ppm and 4.5 ppm, indicating no oxidation occurred. b) Time-resolved FTIR of v$_8$PAO exposed to air over a period of 7 days, revealing no evolution of oxidation peaks, such as O-H around 3500 cm^{-1}. c) Time-resolved FTIR of polyene exposed to air over a period of 7 days. Note the O-H stretch intensity at 3500 cm^{-1} increased and plateaued after 1 day.

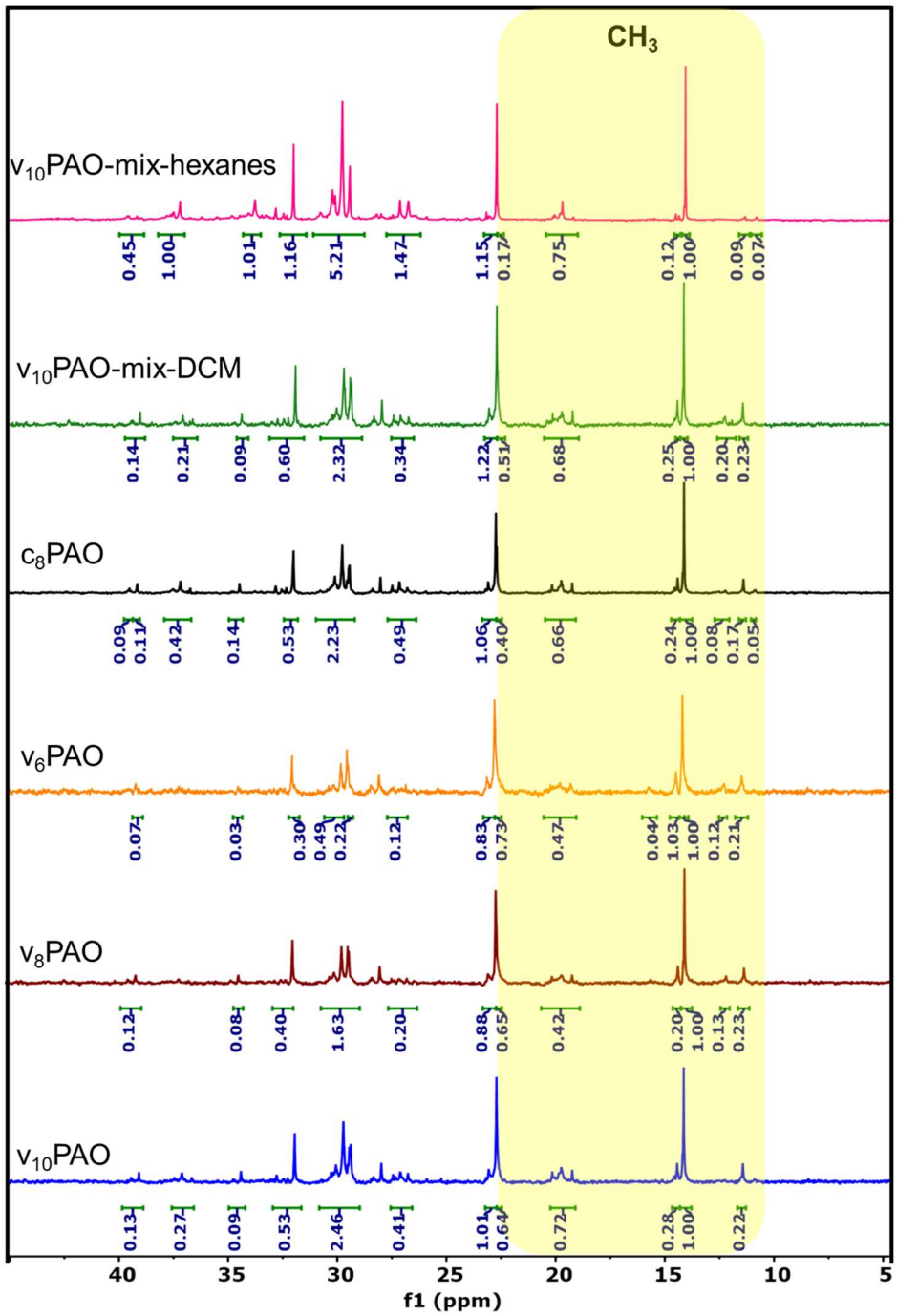

Figure S2. Integration of ^{13}C NMR peaks to evaluate the branching ratio in vPAO. All vPAO lubricants were synthesized in DCM except v_{10}PAO-mix-hexanes. CH_3 signals, 10.8-22.7 ppm; CH_2 signals, 22.7-44 ppm (negative signals in DEPT 135). The mixed PVC waste consisted of cards, gloves, pipes, and toy frogs.

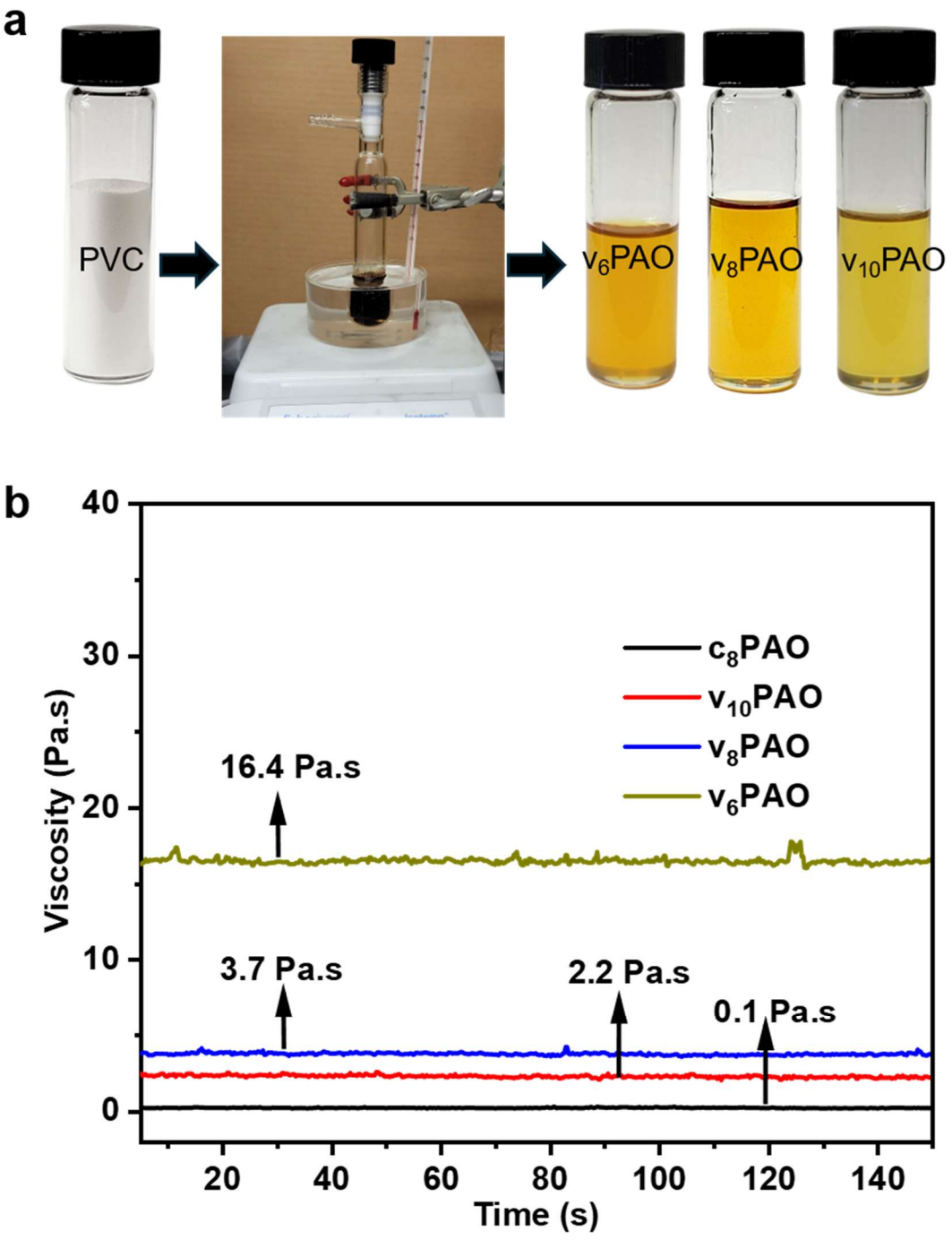

Figure S3. a) Photographs show the PVC powder, reaction setup, and vPAO products. b) Effect of α-olefin chain length on the vPAO dynamic viscosity at 20 °C. Longer-chain α-olefins resulted in lower dynamic viscosities at room temperature.

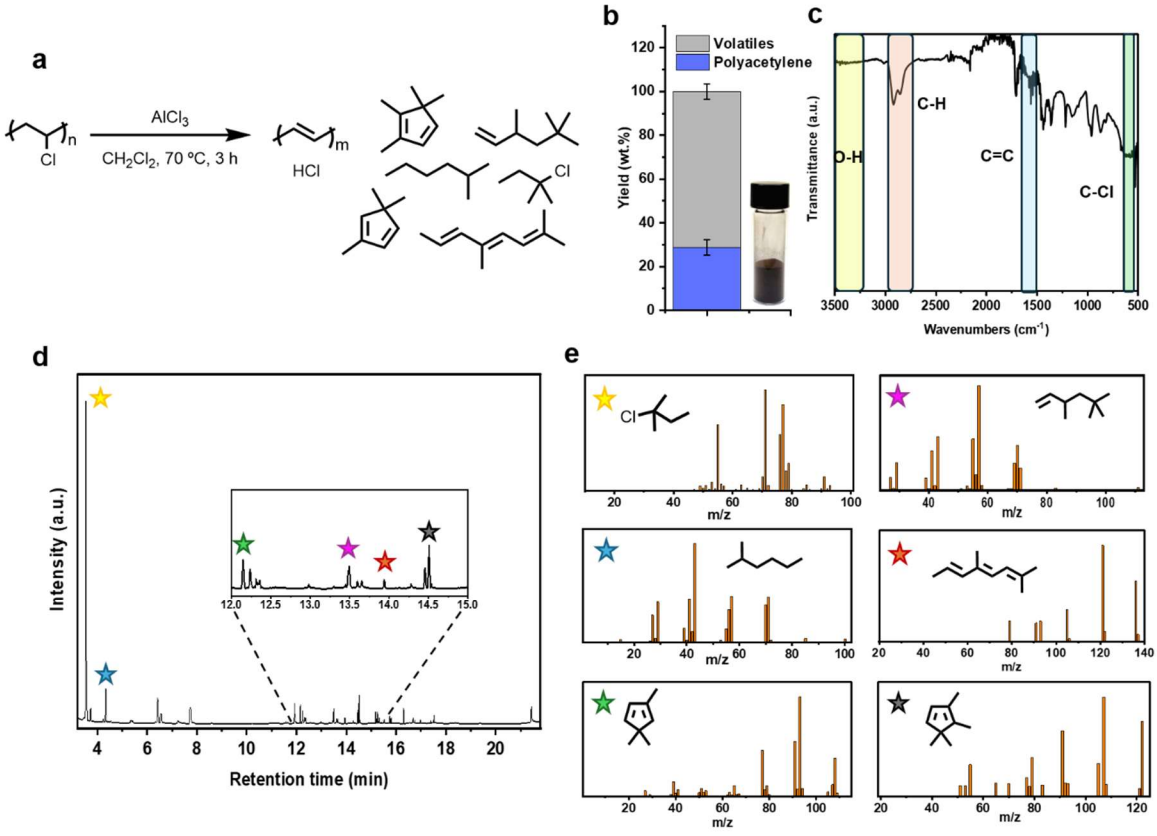

Figure S4. Effect of alpha-olefins in PVC upcycling. a) Scheme of PVC reaction without α-olefins, producing polyenes, cyclopentadienes, chlorohydrocarbons, and other molecules. b) reaction product phase breakdown. c) FTIR of the solid phase. d) GC trace and e) MS spectra of the liquid phase, showing t-amyl chloride as the predominant product.

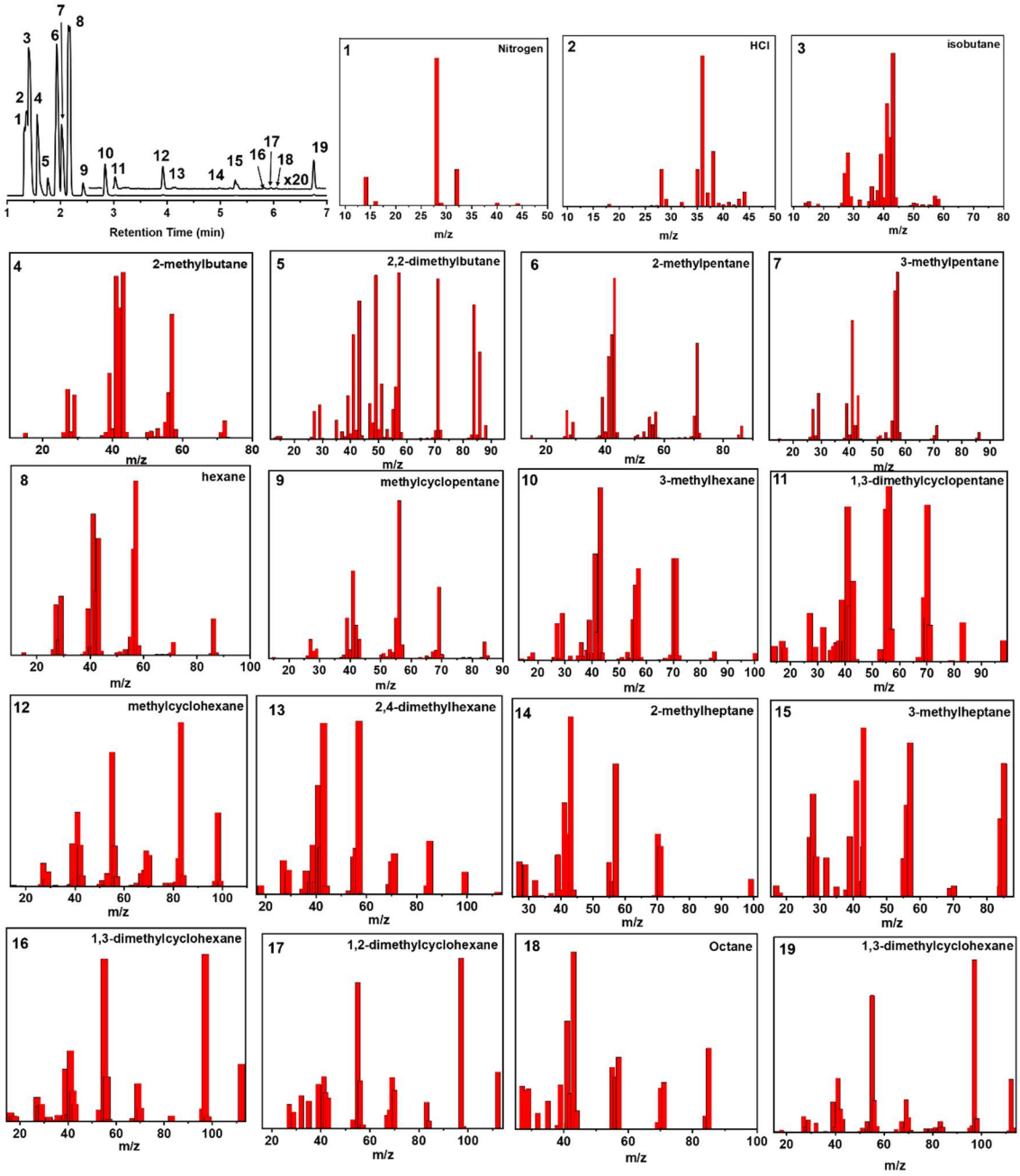

Figure S5. GC-MS analysis of the gas phase of v8PAO synthesis in hexanes. The product stream consisted mostly of isoalkanes and naphthenes. No unsaturated hydrocarbons were detected.

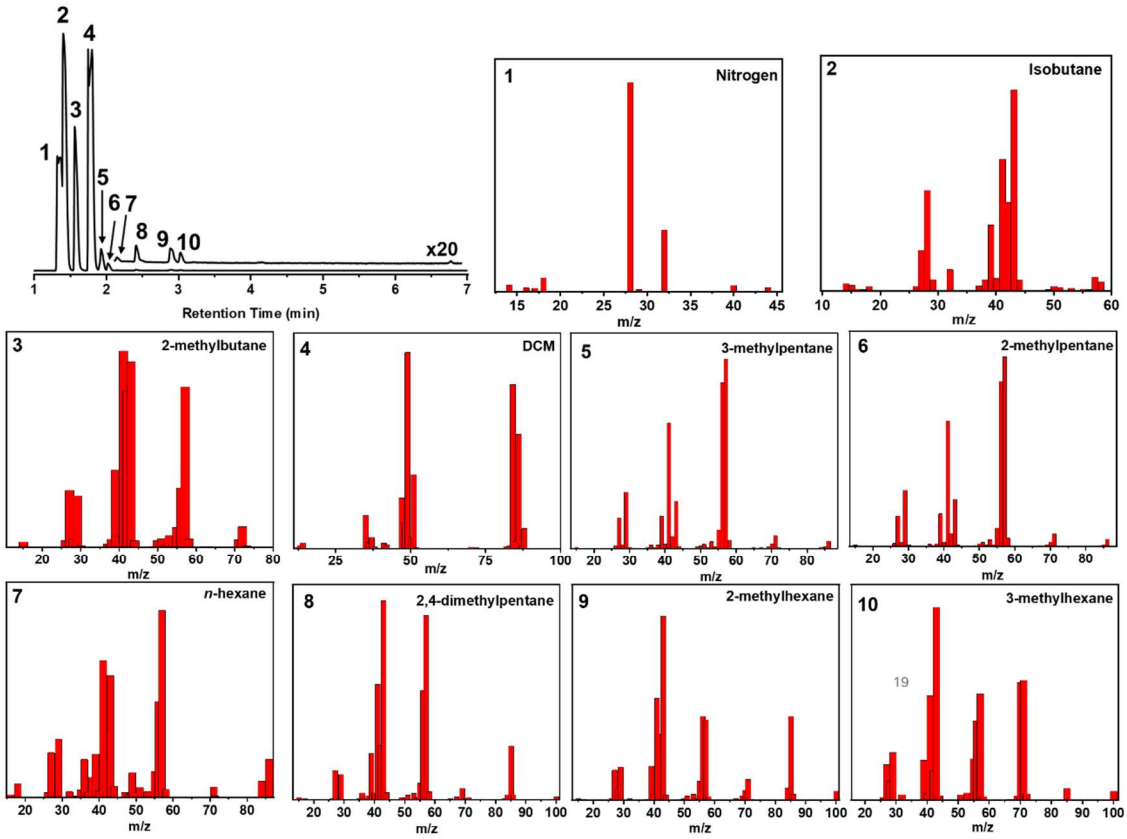

Figure S6. GC-MS analysis of the gas phase of v_8PAO synthesis in DCM. The reaction generated mostly isoalkanes, similar to the upcycling reactions in hexanes.

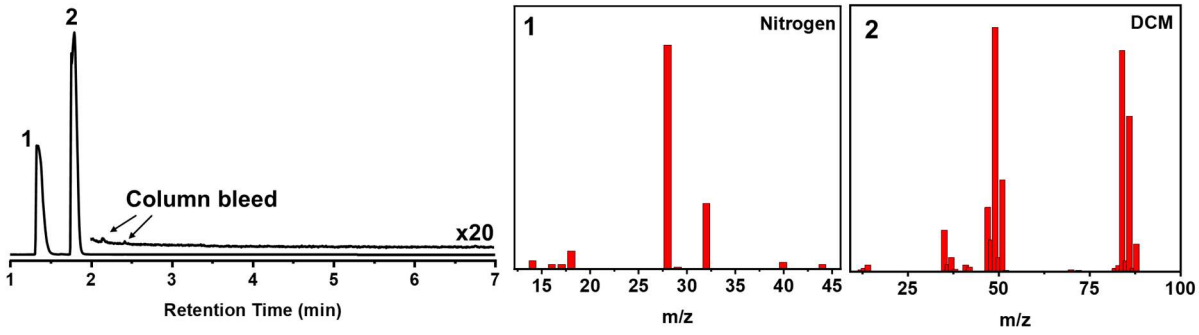

Figure S7. GC-MS analysis of the gas phase of the control reaction in DCM. No hydrocarbon gaseous products were observed. Low-molar-mass molecules from PVC degradation likely remained in the solvent DCM.

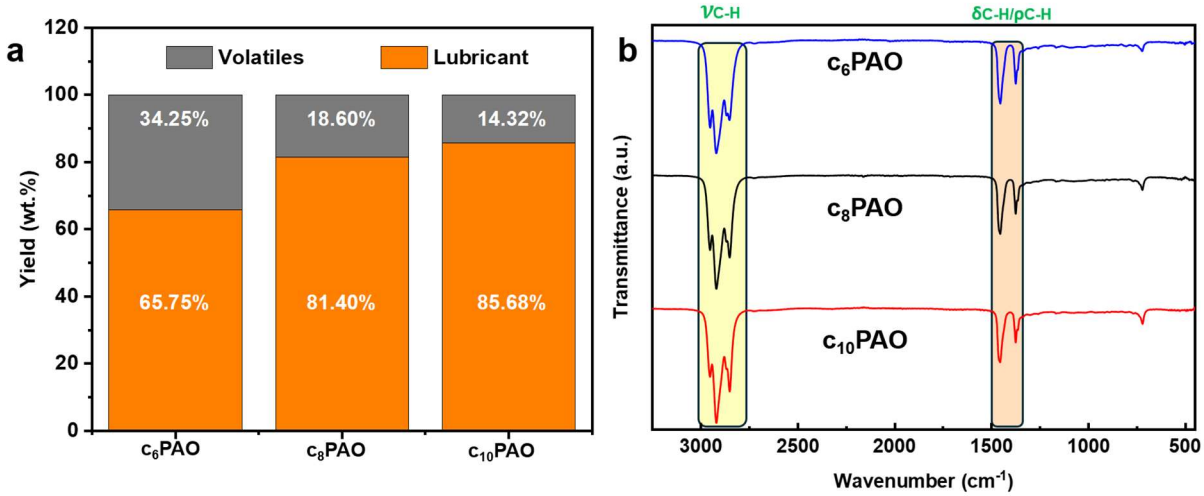

Figure S8. **Control reactions of α-olefin oligomerization without PVC**. a) The yield of cPAO lubricants increased with an increasing α-olefin chain length from 1-hexene to 1-decene. b) FTIR spectra of cPAO show the signals pertinent to C-H bonds.

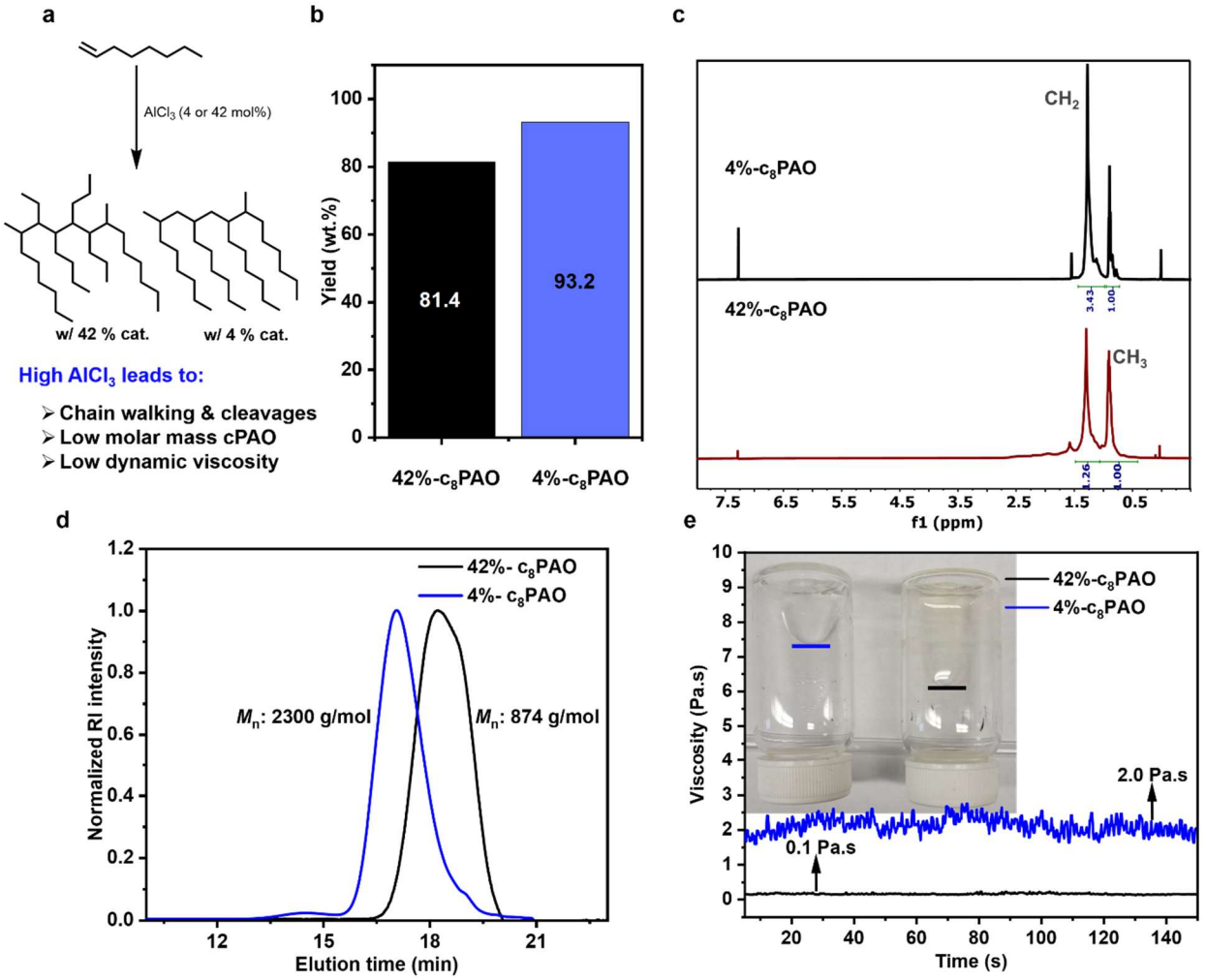

Figure S9. Effect of $AlCl_3$ loading on the molar mass and viscosity of cPAO. a) Reaction scheme of 1-octene oligomerization using $AlCl_3$ catalyst, b) cPAO yield under the two $AlCl_3$ loadings, c) ^1H NMR spectra show CH_2/CH_3 integration ratios, indicating fewer branches for cPAO synthesized at 4% $AlCl_3$ (4%-c_8PAO) than 42% loading (42%-c_8PAO). Note: In this control experiment, the $AlCl_3$ loading is with respect to the alkene content. In other words, the weight of $AlCl_3$ is the same in control reactions (42 mol% $AlCl_3$ loading with respect to alkene) as that in the upcycling reaction (50 mol% $AlCl_3$ with respect to PVC). d) SEC traces show that 4%-c_8PAO had a higher molar mass than 42%-c_8PAO, e) 4%-c_8PAO exhibited a dynamic viscosity about one order of magnitude higher than 42%-c_8PAO. (inset) digital photographs of 4%-c_8PAO and 42%-c_8PAO.

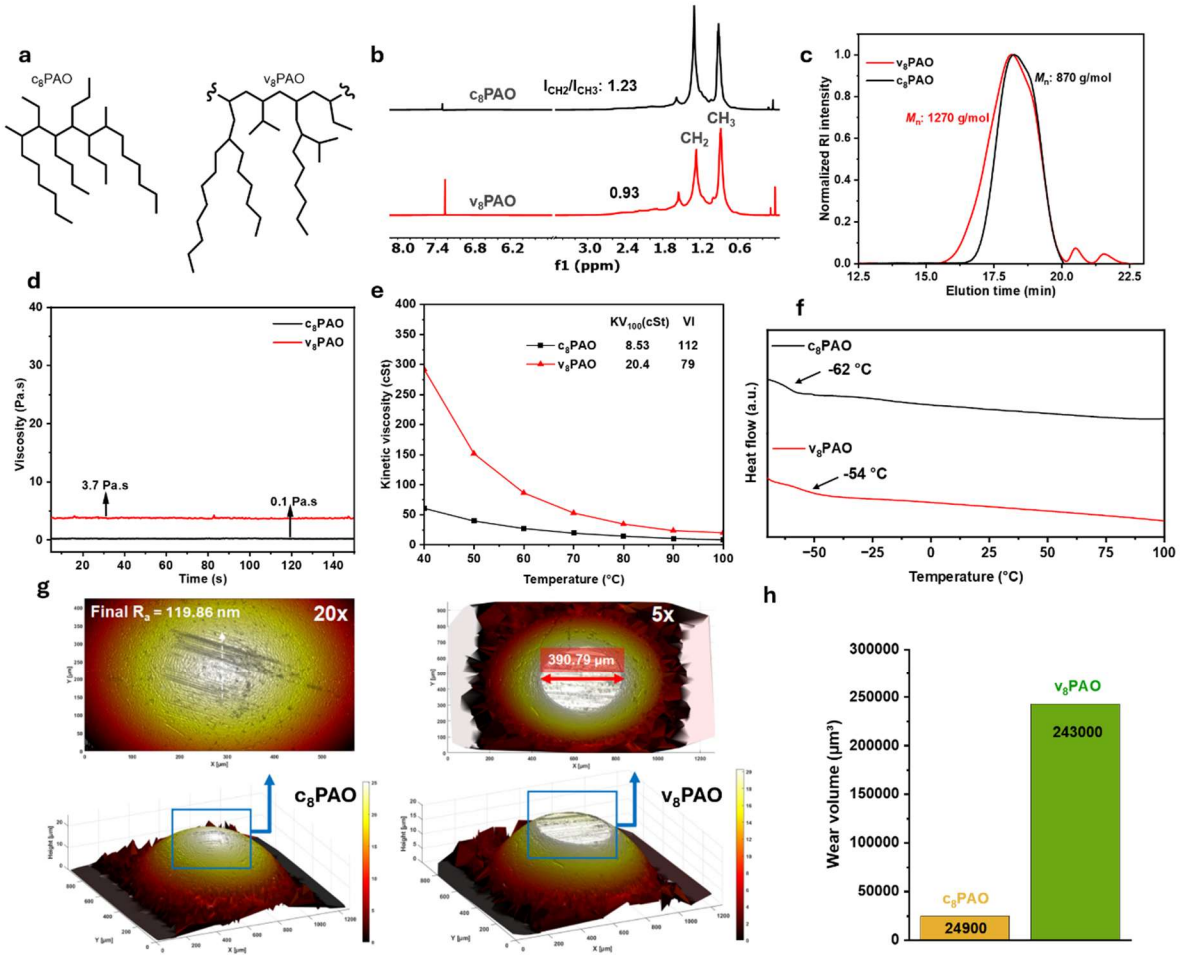

Figure S10. Lubricant properties of α-olefin reactions with and without PVC. a) Structures of c_8PAO and v_8PAO synthesized in DCM, comparing the extent of branching and branching chain lengths. b) ^{1}H NMR of c_8PAO and v_8PAO displaying the degree of branching determined through the I_{CH2}/I_{CH3} integral ratios. c) SEC chromatograms of c_8PAO and v_8PAO. d) dynamic viscosity and e) kinematic viscosity of c_8PAO and v_8PAO, revealing high viscosity for the more branched v_8PAO at low temperatures. f) DSC thermograms of c_8PAO and v_8PAO showing high T_g for the PVC-derived lubricant. g) 3D profiles of the ball's contour after tribology tests. v_8PAO resulted in a deep scar due to poor lubrication performance of short branch chains, whereas c_8PAO led mostly to abrasion marks. h) Wear volume of scars incurred in tribology experiments.

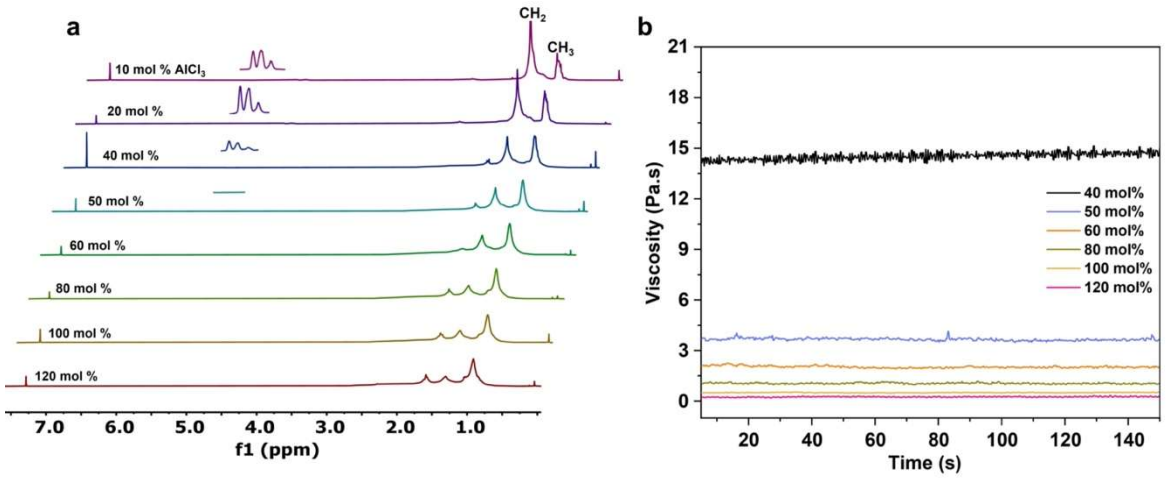

Figure S11. Structural analysis and viscosity measurement of upcycled products under an increasing $AlCl_3$ loading. a) ^1H NMR in $CDCl_3$ of v_8PAO prepared under various $AlCl_3$ loading (from 10 mol% to 120 mol%). The reactions were run in DCM. During ^1H NMR characterization, the v_8PAO prepared at 10 mol% loading was mostly PVC-like and exhibited poor solubility in $CDCl_3$. b) Dynamic viscosities of v_8PAO prepared under various $AlCl_3$ loading (from 40 mol% to 120 mol%). At $AlCl_3$ loadings of 10 mol% and 20 mol%, the product was too greasy to be recorded by the rheometer used in this study.

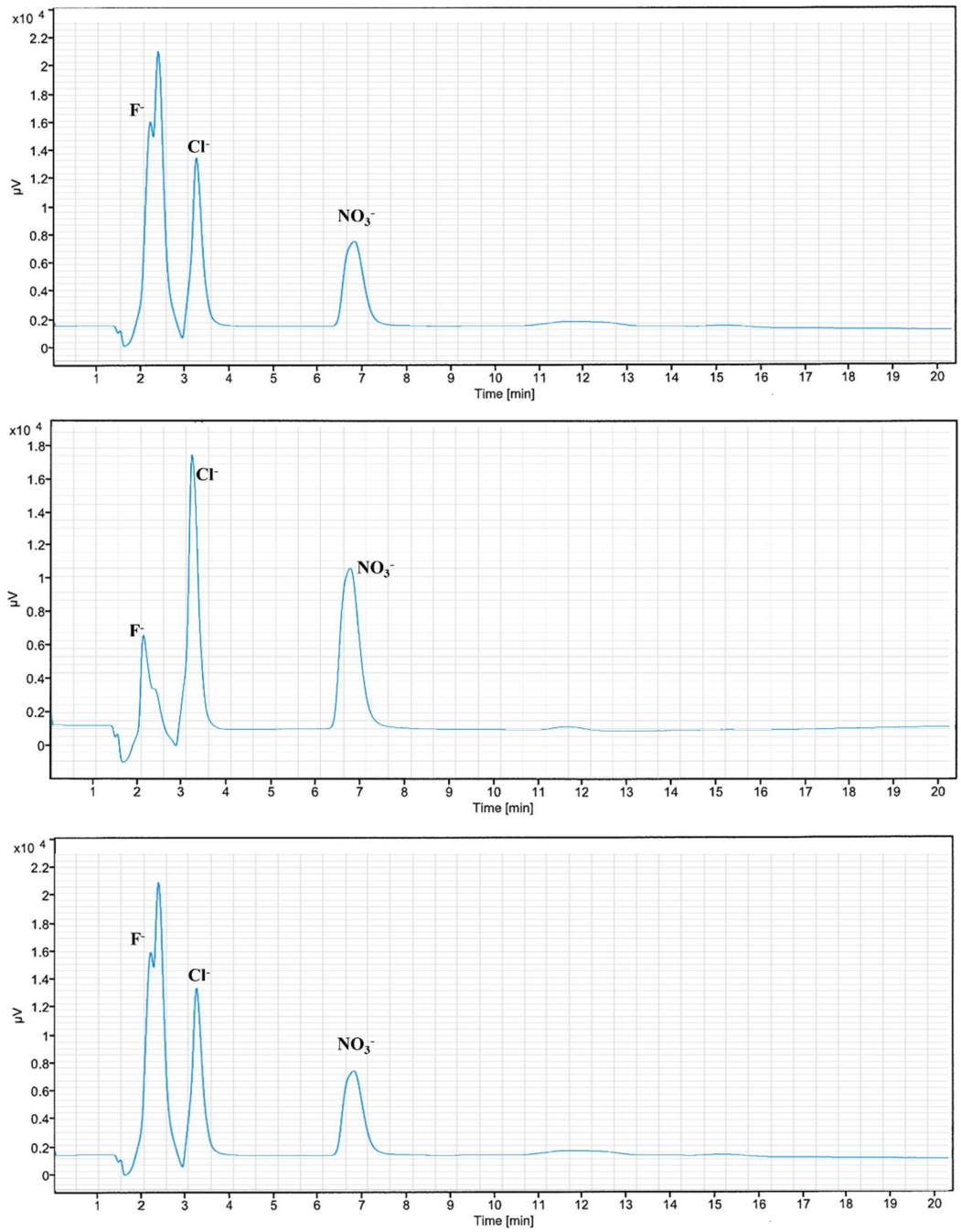

Figure S12. Ion chromatograms reveal chlorine in the oils. Top: v_8PAO; middle: v_{10}PAO-mix-DCM; bottom: v_{10}PAO-mix-hexanes. The concentration of chlorine in all oil samples was < 100 ppm.

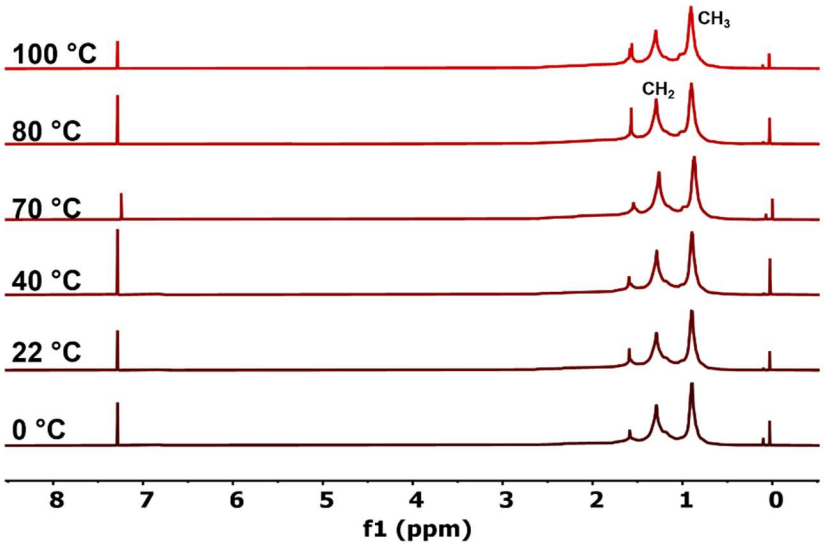

Temperature (°C)	I_{CH2}/I_{CH3}
100	0.71
80	0.88
70	0.93
40	0.93
22	0.96
0	0.98

Figure S13. ^{1}H NMR in $CDCl_3$ of lubricants synthesized at varying temperatures. The degree of branching increased with the reaction temperature, as evidenced by the ratio of I_{CH2}/I_{CH3}.

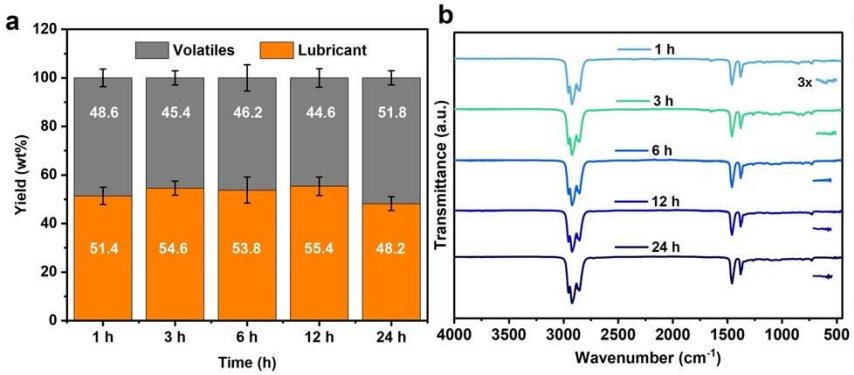

c

Time (h)	Yield (wt%)	M_n (g/mol)
1	51.4	1,410
3	54.6	1,270
6	53.8	1,620
12	55.4	1,570
24	48.2	1,490

Figure S14. Reaction time optimization. a) Product yield at various reaction time durations from 1 h to 24 h. b) FTIR spectra of the lubricants. Only the 1-h reaction showed residual C-Cl bonds. c) Summary of the yield and molar mass of lubricants as a function of reaction time.

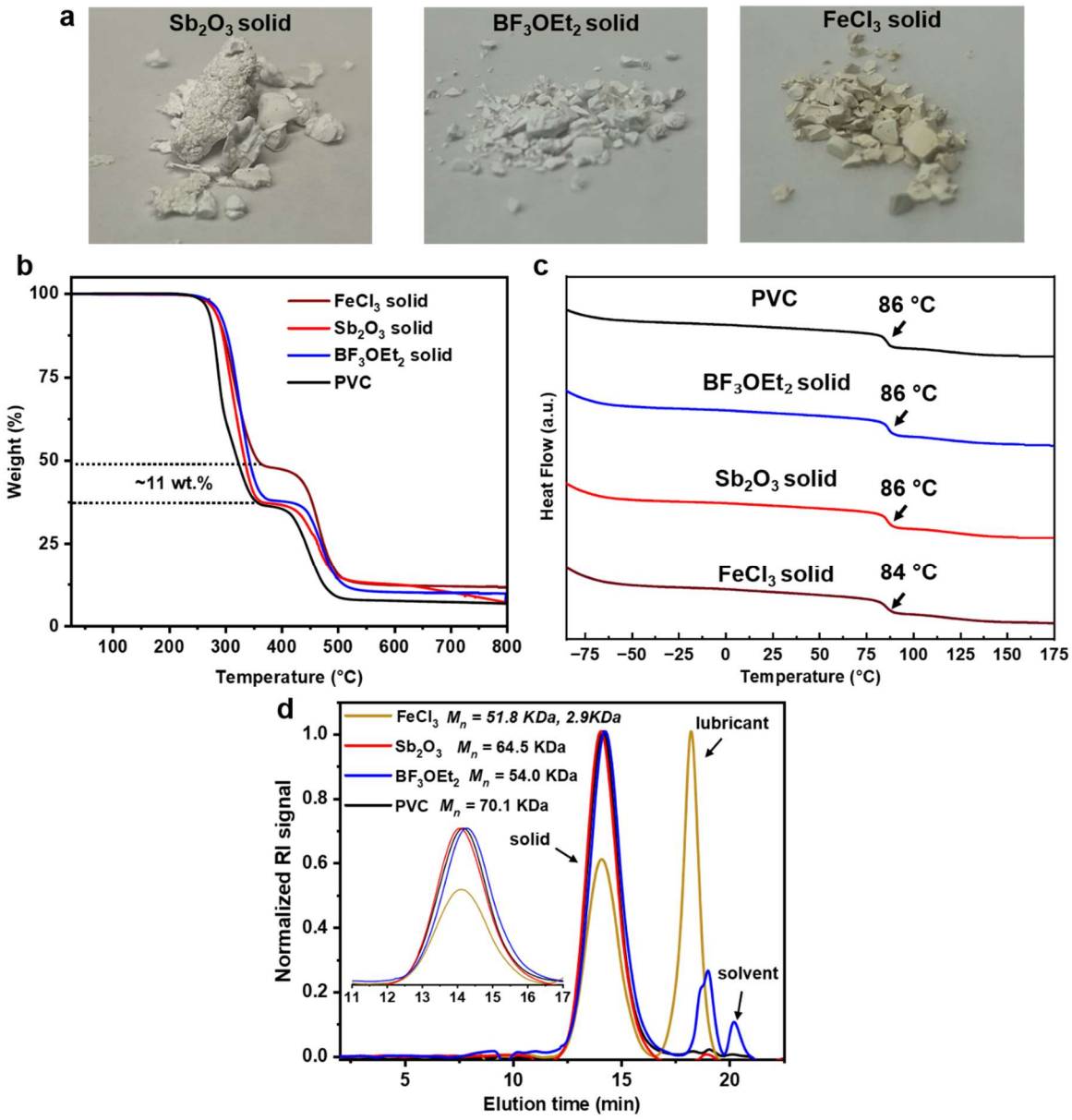

Figure S15. Analysis of by-products from PVC upcycling reactions using alternative Lewis acids. a) Digital photographs of recovered solids after the reaction. b) TGA and c) DSC thermograms of solids showing a slight drop in the T_g of $FeCl_3$ solid byproduct. d) SEC traces of solid products indicate a slight decrease in molar mass compared to virgin PVC. The reaction with $FeCl_3$ produced limited quantities of lubricants. These analyses suggest that the solids might be partially alkylated PVC, and the degree of alkylation depended on the Lewis acid used in the reaction.

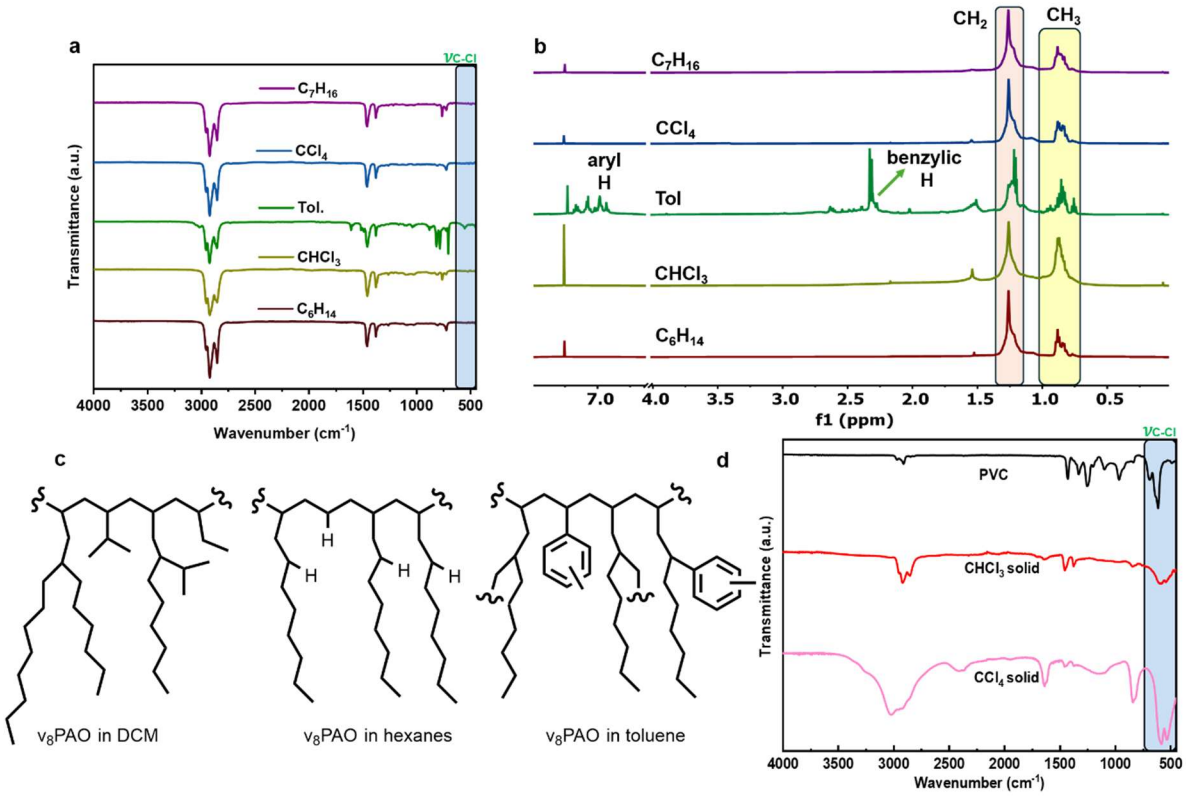

Figure S16. Upcycling of PVC in alternative solvents. a) FTIR analysis of v_8PAO lubricants obtained from various solvents, b) ^{1}H NMR of v_8PAO lubricants in $CDCl_3$, c) plausible chemical structures of vPAO prepared in chlorinated, hydrocarbon, and aromatic solvents, d) FTIR of solid by-products exhibiting strong C-Cl signals.

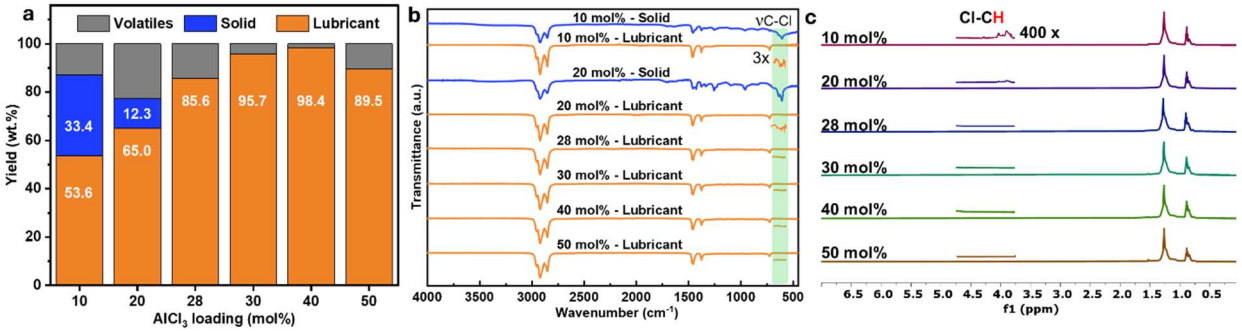

Figure S17. Optimization of $AlCl_3$ loading in PVC upcycling reactions in hexanes. a) Product yield at various $AlCl_3$ loadings. b) FTIR spectra of the lubricants and solids formed as the $AlCl_3$ loading varies. c) ^1H NMR spectra of the lubricants showing hydrogen signals at 4.0 ppm in the 10 mol% loading sample, likely corresponding to methine hydrogen near the Cl in low molar mass chlorohydrocarbons[45].

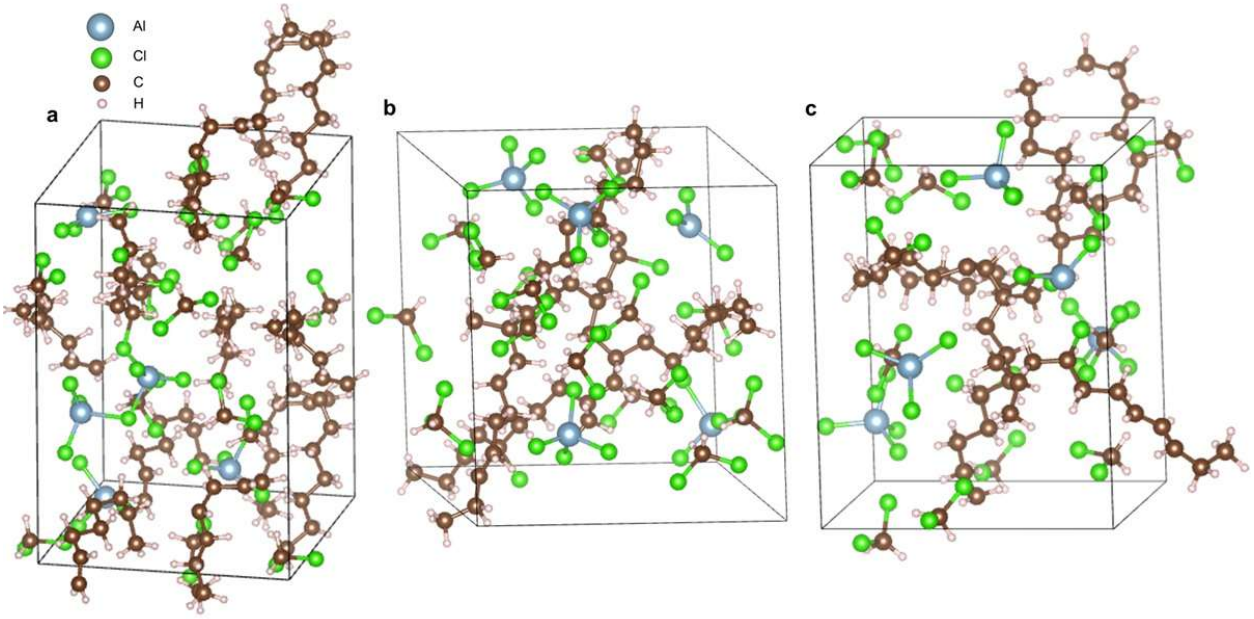

Figure S18. **Representation of the simulation cells containing all the atoms.** a) Initial structure containing atactic PVC chain with five monomers, five 1-octene, five $AlCl_3$, and ten DCM molecules. b) Five 1-octene molecules are attached to the five active sites in parallel, forming a "comb-like" structure. c) Five 1-octene molecules are oligomerized and attached to one active site, forming a "branch-like" structure.

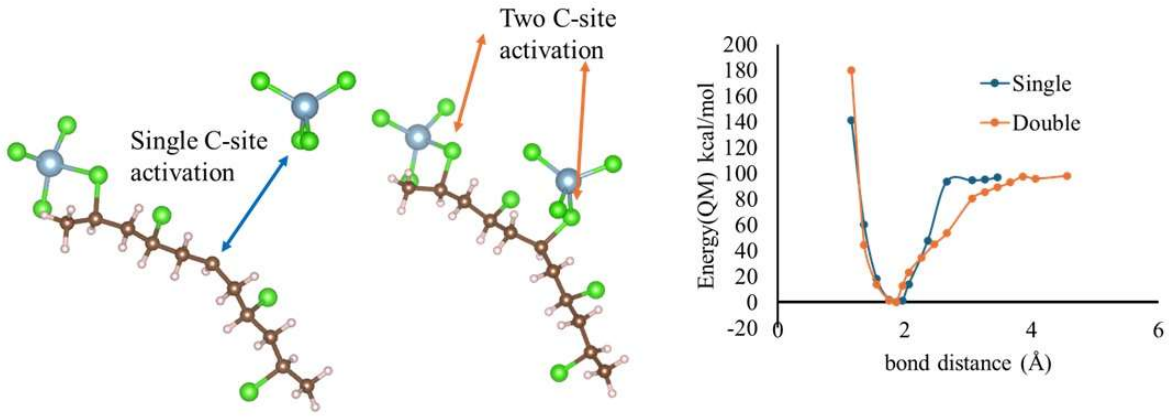

Figure. S19. Comparison of the relative energetics of a single Cl-site (left) and double Cl-sites (right) on PVC. $AlCl_3$ forms $AlCl_4^-$ after binding to Cl on PVC, and $AlCl_4^-$ is cleaved, forming an active carbon site on PVC in a gas-phase reaction. The energy comparison plot shows the DFT-calculated bond-breaking energy of ~96 kcal/mol in both simulated cases.

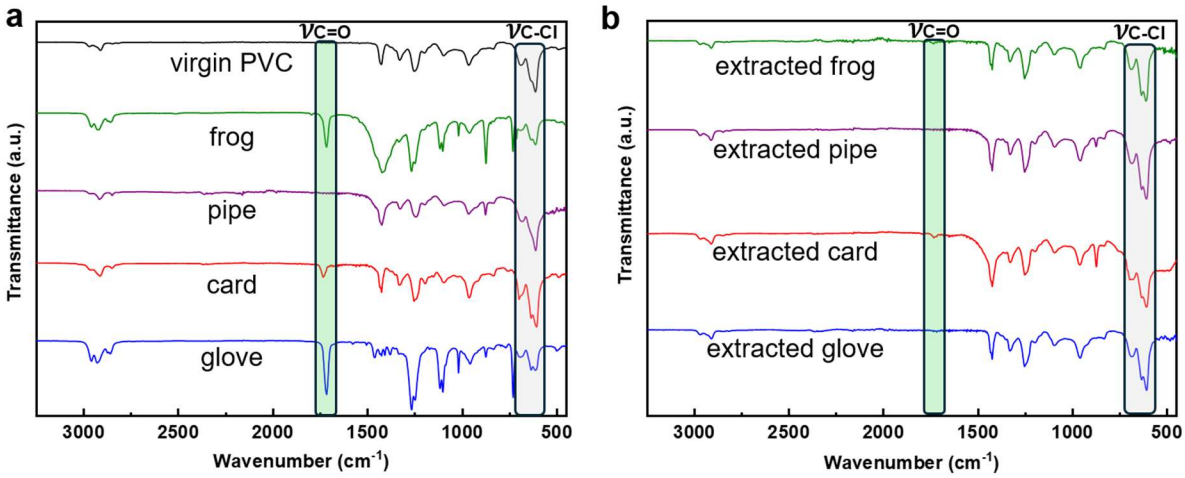

Figure S20. Extraction of PVC from real-world products. a) FTIR spectra of PVC products as received. b) FTIR spectra of extracted PVC.

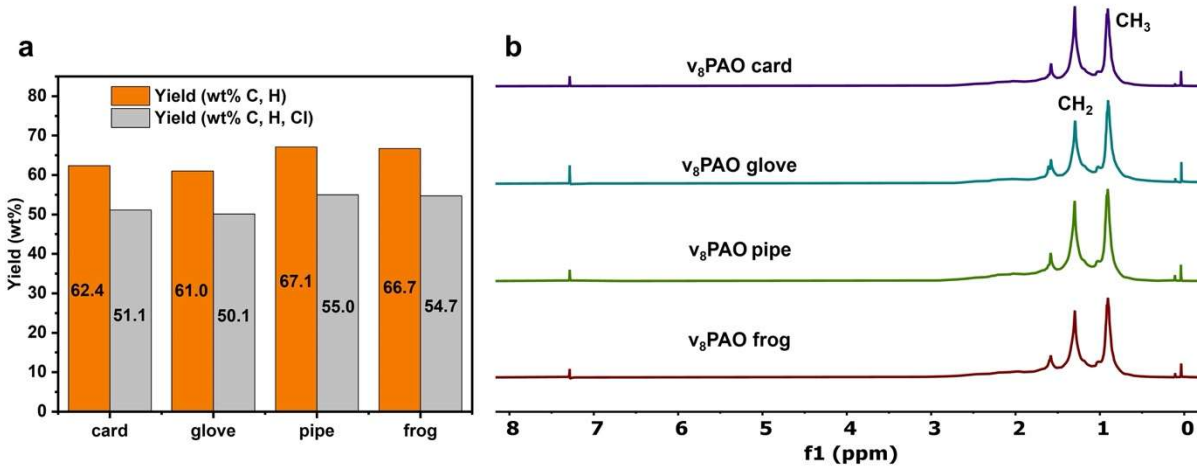

Figure S21. Upcycling of PVC waste to v8PAO. a) Yields of the lubricants on a basis of C and H (orange bars) and the total mass of C, H, and Cl (gray bars). b) ^{1}H NMR of the lubricants from various types of PVC waste.

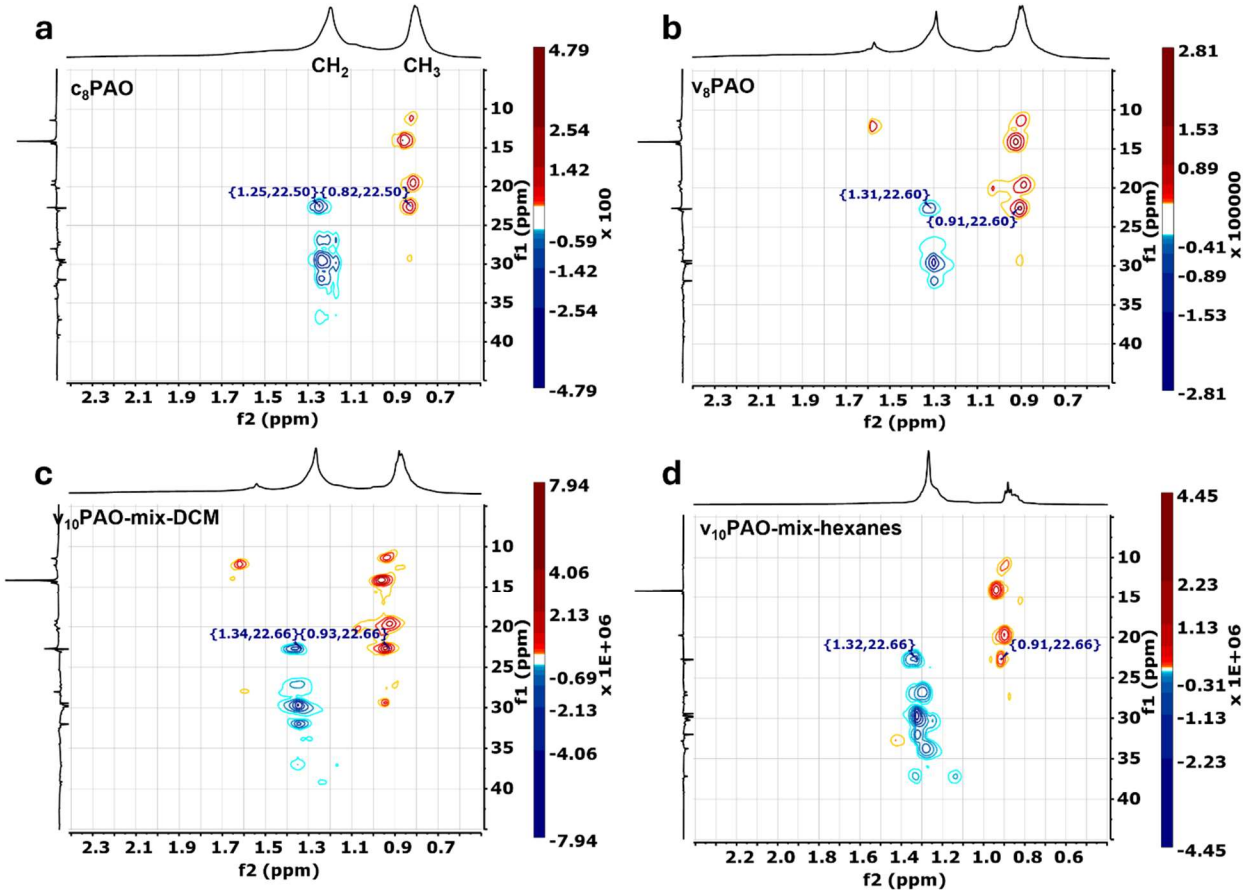

Figure S22. HSQC spectra of the oils. a) HSQC of c_8PAO alkyl region, b) v_8PAO, c) v_{10}PAO-mix-DCM, and d) v_{10}PAO-mix-hexanes showing the correlation intensity map of β-CH_2 and isopropyl type CH_3 signals at ~22.6-22.9 ppm in ^{13}C NMR. The strength of the methyl group cross-peak showcases the difference in branching between oils prepared in DCM and hexanes.

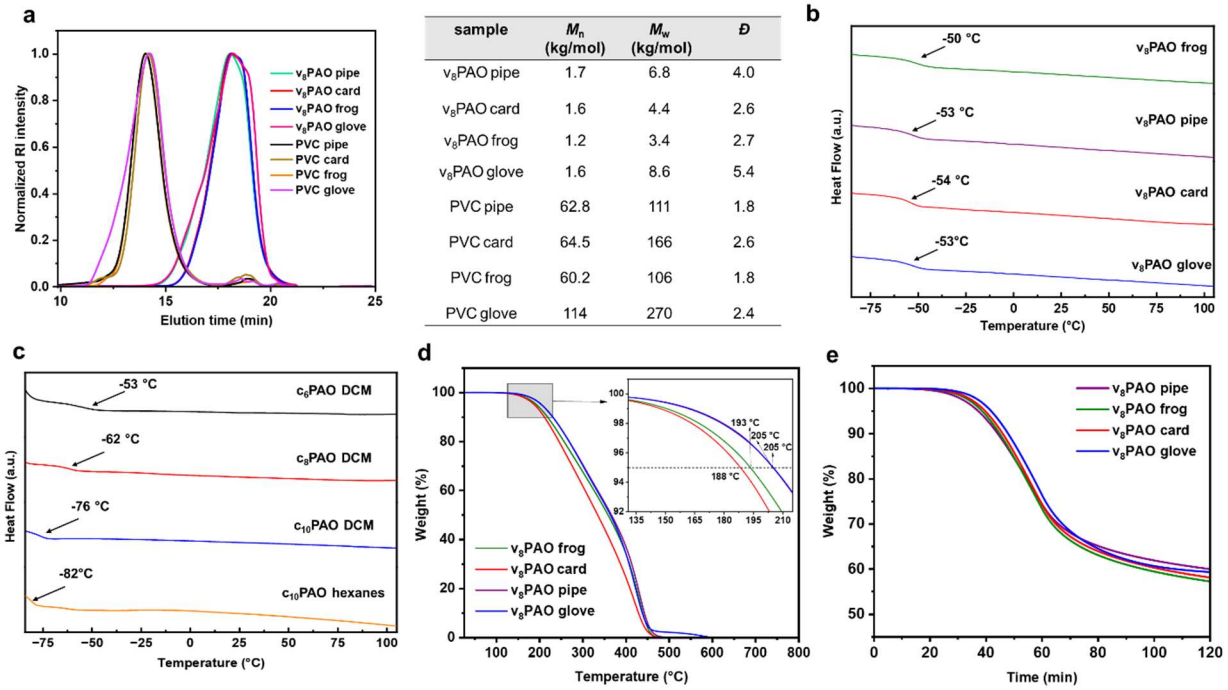

sample	M_n (kg/mol)	M_w (kg/mol)	$Đ$
v_8PAO pipe	1.7	6.8	4.0
v_8PAO card	1.6	4.4	2.6
v_8PAO frog	1.2	3.4	2.7
v_8PAO glove	1.6	8.6	5.4
PVC pipe	62.8	111	1.8
PVC card	64.5	166	2.6
PVC frog	60.2	106	1.8
PVC glove	114	270	2.4

Figure S23. Molar mass and thermal properties of waste-derived lubricants synthesized in DCM. a) SEC chromatograms and molar masses of various PVC feedstocks and the corresponding v**8**PAO synthesized in DCM. b) DSC of v**8**PAO showing glass transition temperatures. c) DSC of cPAO prepared using 1-hexene, 1-octene, and 1-decene in a solvent of either DCM or hexanes. d) TGA thermograms of v**8**PAO synthesized from various types of PVC waste. All lubricants showed $T_{d5\%}$ >180 °C. e) ASTM D5800 test of v**8**PAO synthesized from various types of PVC waste (28 - 250 °C at 3.7 °C/min followed by an isothermal hold at 250 °C for 60 min under an air environment).

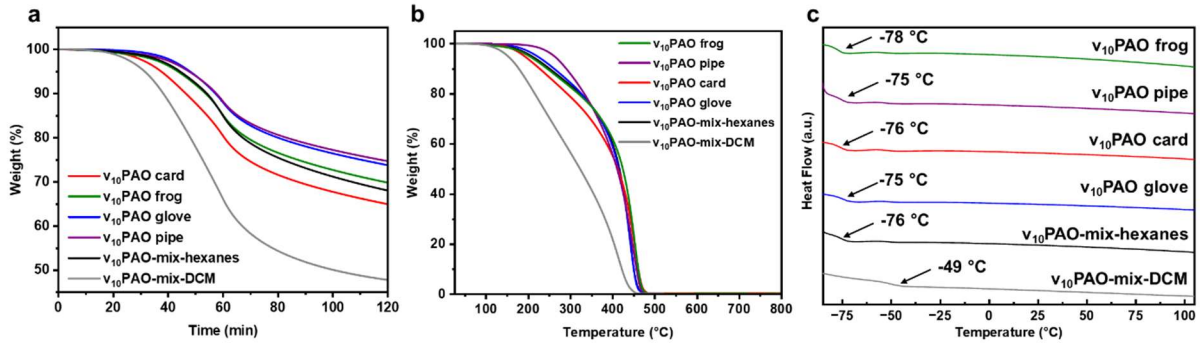

Figure S24. Thermal properties of waste-derived vPAO$_{10}$ synthesized in hexanes and comparison with their counterparts synthesized in DCM. a) ASTM D5800 test thermogram demonstrating residual weight for lubricants synthesized in hexanes higher than that in DCM. b) TGA thermograms and c) DSC thermograms displaying low T_g for hexanes system, likely due to minimal branching.

Avg COF ± std		
SAMPLE	25 °C	60 °C
v_{10}PAO-mix-hexanes	0.085 ± 0.009	0.074 ± 0.008
PAO40	0.074 ± 0.006	0.074 ± 0.008
PAO10	0.089 ± 0.007	0.102 ± 0.007

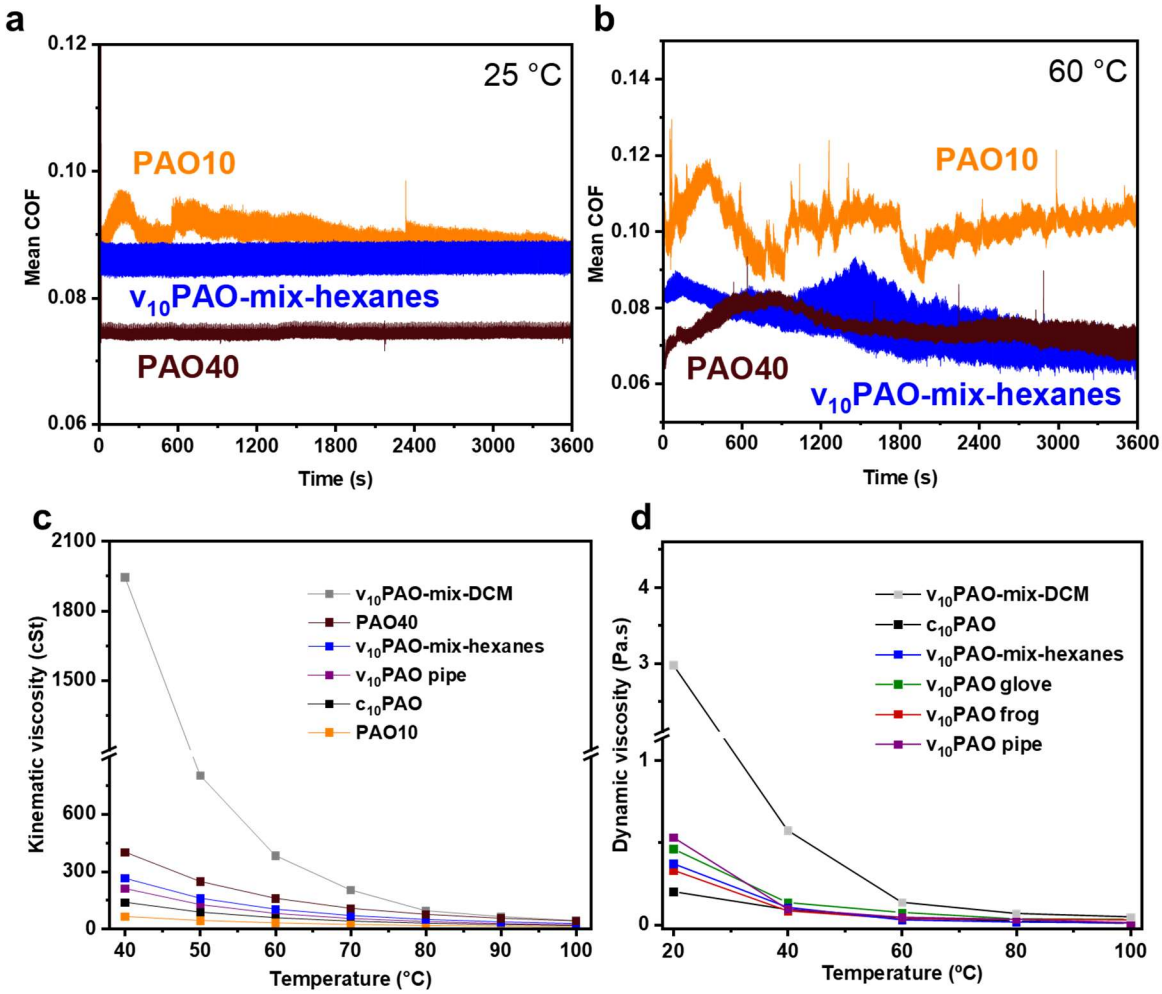

Figure S25. Tribology and viscosities of waste-derived v_{10}PAO. a) Coefficient of friction (COF) of v_{10}PAO from a mixed waste stream synthesized in hexanes, compared with that of commercial PAO10 and PAO40 at 25 °C and b) 60 °C. c) Kinematic viscosity and d) dynamic viscosity of v_{10}PAO from various waste, compared with the standard commercial PAO10 lubricant.

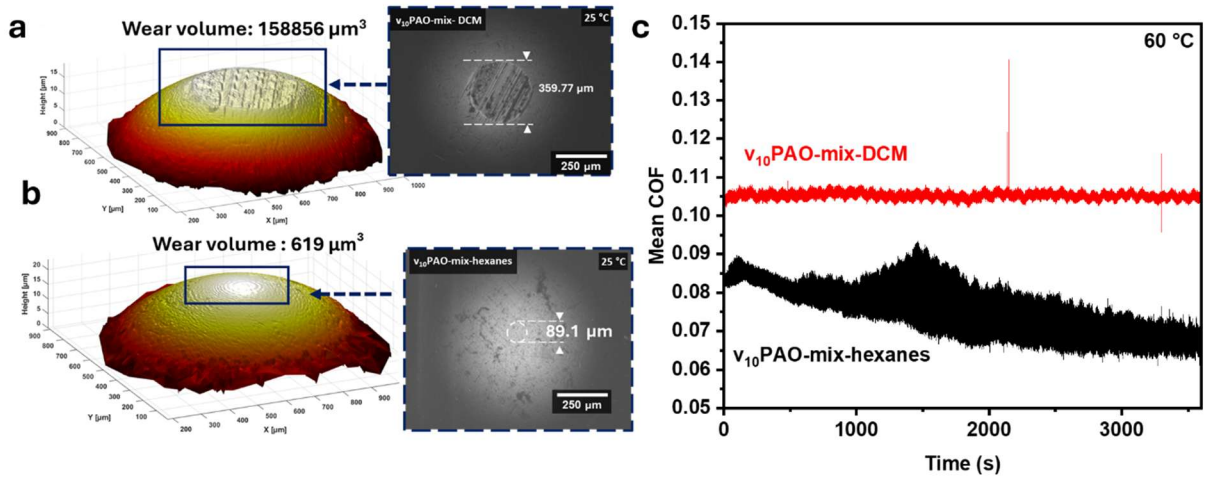

Figure S26. Comparative tribological performance of v_{10}PAO-mix-DCM and v_{10}PAO-mix-hexanes. 3D profiles of the steel ball after tribology test of oils: a) v_{10}PAO-DCM and b) v_{10}PAO-hexanes, showing the change in scar wear volume. The wear volume of the v_{10}PAO-DCM oil was higher than that of v_{10}PAO-hexanes, demonstrating the effect of the lubricant microstructure on tribological performance. c) Coefficient of friction of v_{10}PAO-DCM and v_{10}PAO-hexanes at 60°C.

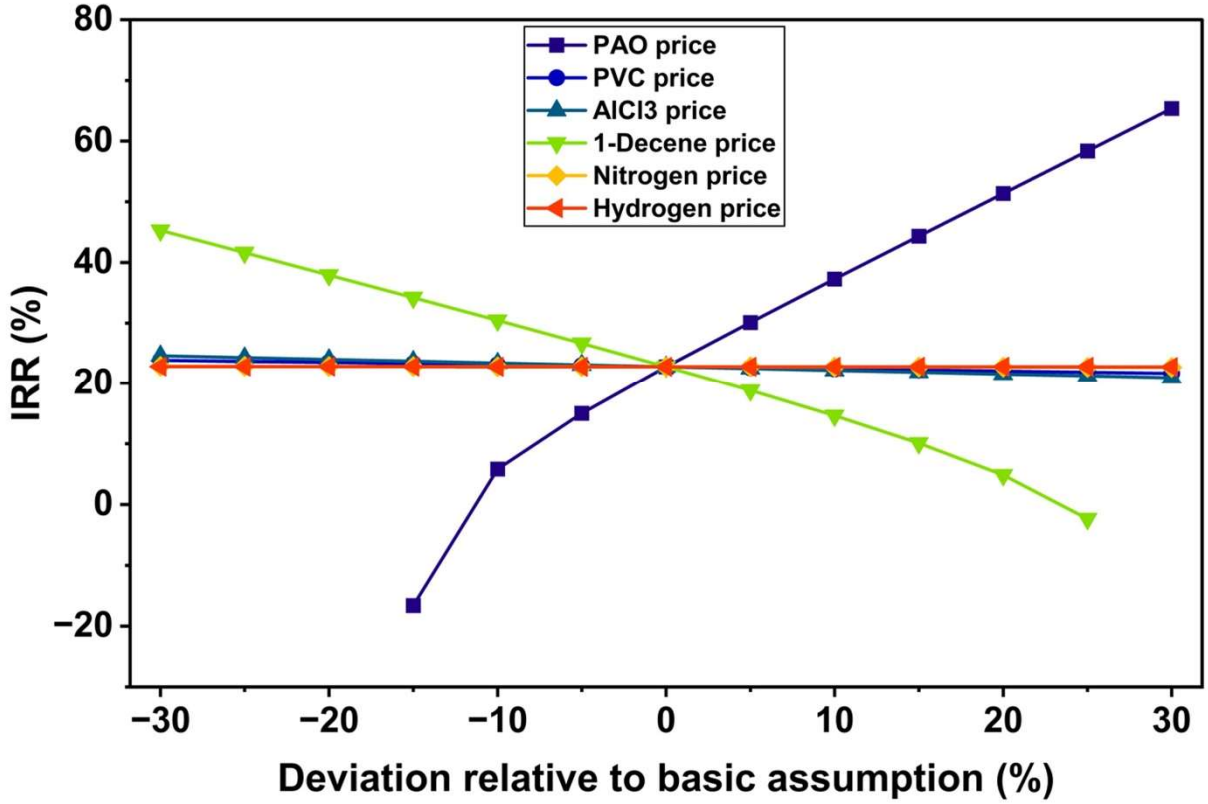

Figure S27. Sensitivity of IRR with respect to prices of raw materials and the product.

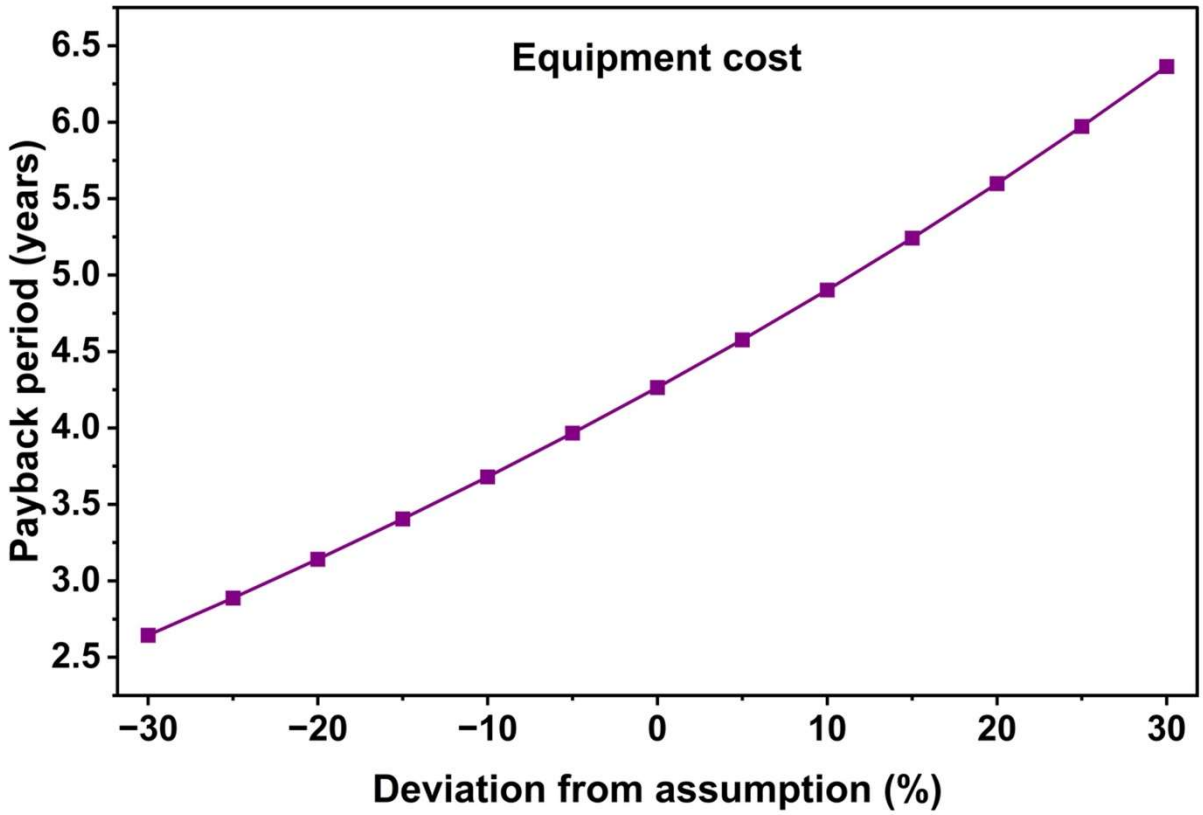

Figure S28. Sensitivity analysis of equipment cost. Sensitivity analysis of payback period (PBP) with respect to equipment cost, ranging from -30% to 30% of the basic assumption.

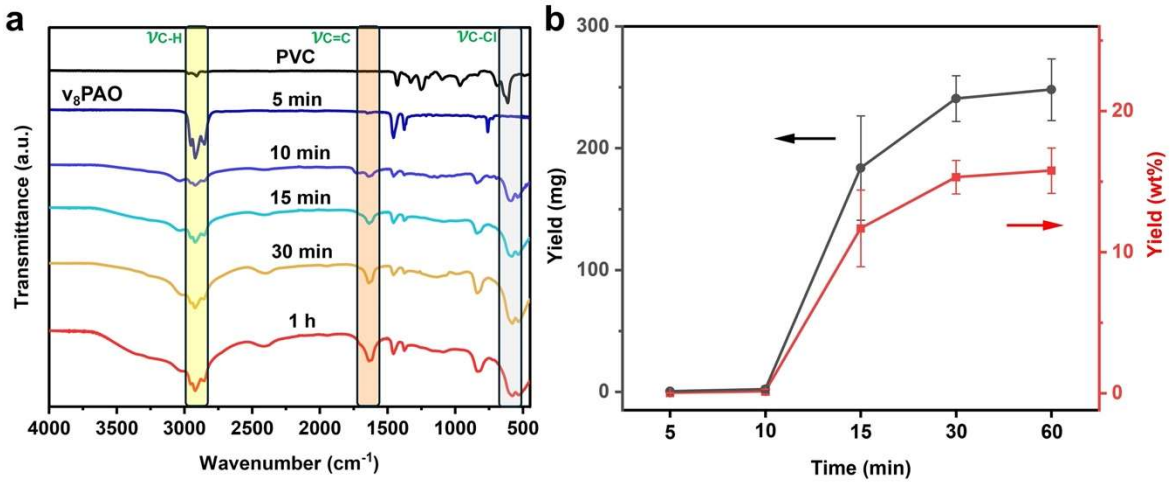

Figure S29. Delayed α-olefin addition to the PVC upcycling reaction. a) FTIR analysis of the major reaction product. The peaks around 1595-1680 cm^{-1} imply that polyacetylene forms in the absence of α-olefin. b) Yield curves of the solid with increasing delay time for a 0.5-g-scale reaction.

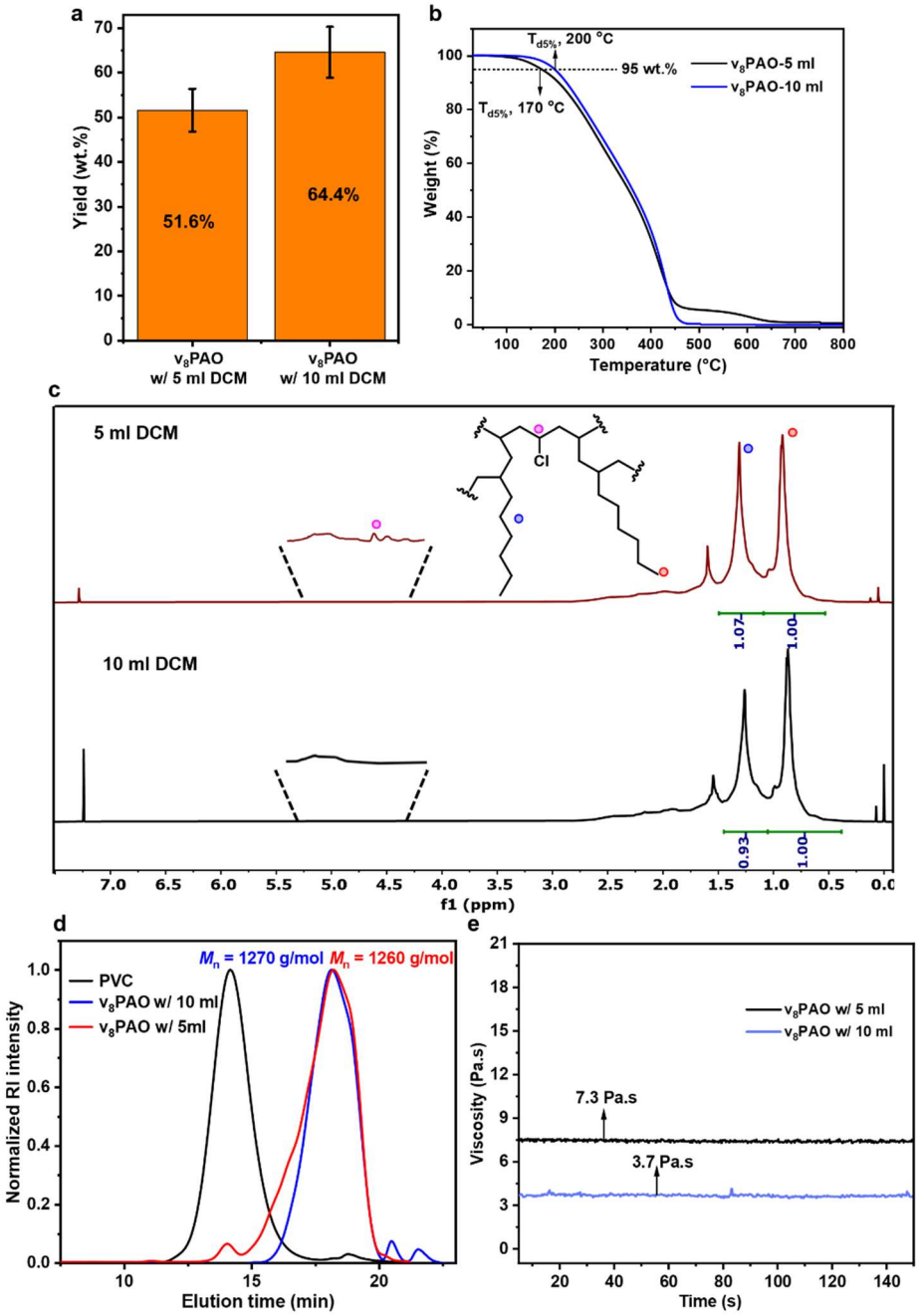

Figure S30. Effect of reactant concentration on v8PAO properties. a) v8PAO yield under two different reaction conditions with varying amounts of DCM solvents. b) TGA thermograms of lubricants show lower $T_{d5\%}$ and less thermal stability for v8PAO prepared under concentrated conditions. c) ^{1}H NMR of lubricant products. The set of peaks centered at ~4.4 ppm is ascribed to protons attached to C-Cl bonds. d) SEC chromatograms reveal a broader dispersity for the v8PAO-5ml lubricant than v8PAO-10mL. e) Rheological measurements show the dynamic viscosities of v8PAO-5ml and v8PAO-10ml.

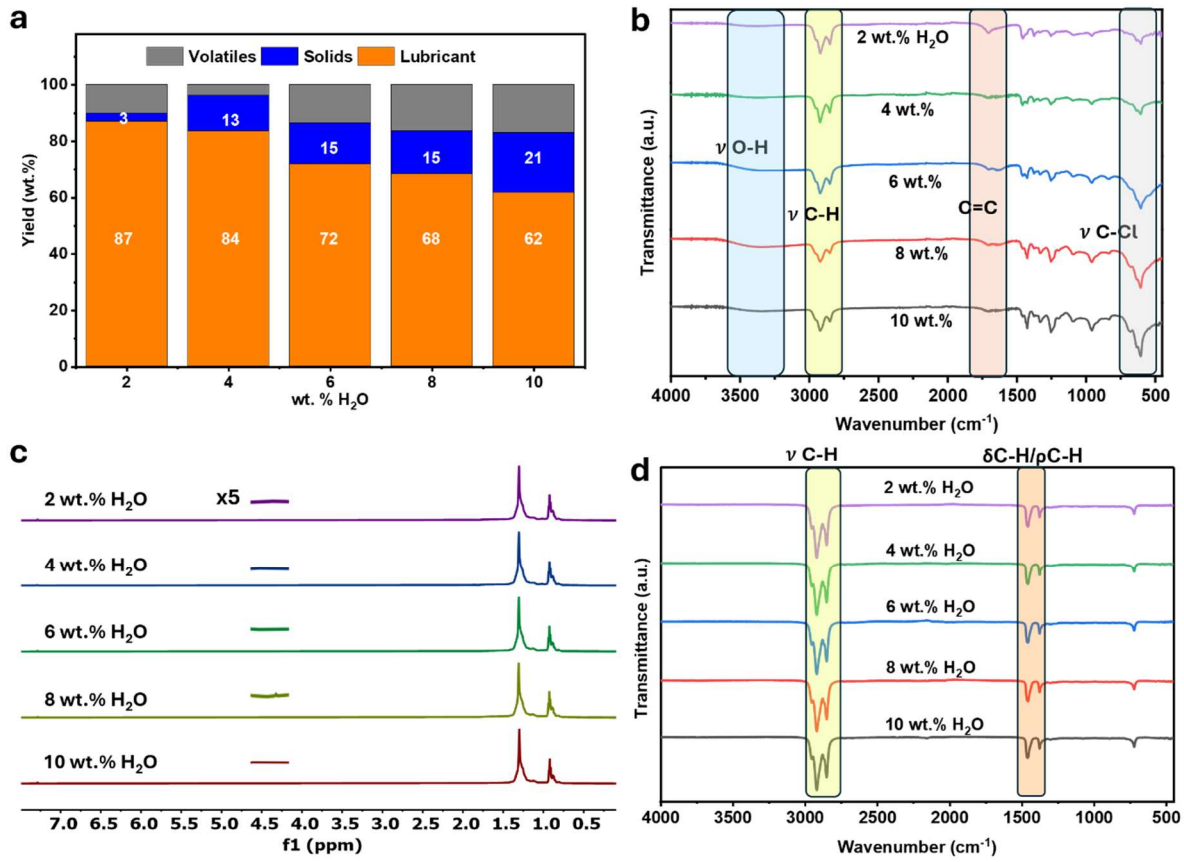

Figure S31. Influence of excess water on the PVC upcycling reaction. a) Product yield at various water contents in the reaction. The water content is based on the mass ratio of water to $AlCl_3$. The yield of solid byproducts increased with water loading, indicating decreased efficiency of $AlCl_3$. b) FTIR spectra of the solids featuring O-H, C=C, and C-Cl peaks as a result of partial dehydrochlorination and dechlorination. c) ^1H NMR and d) FTIR spectra of the lubricants showing no detectable C-Cl.

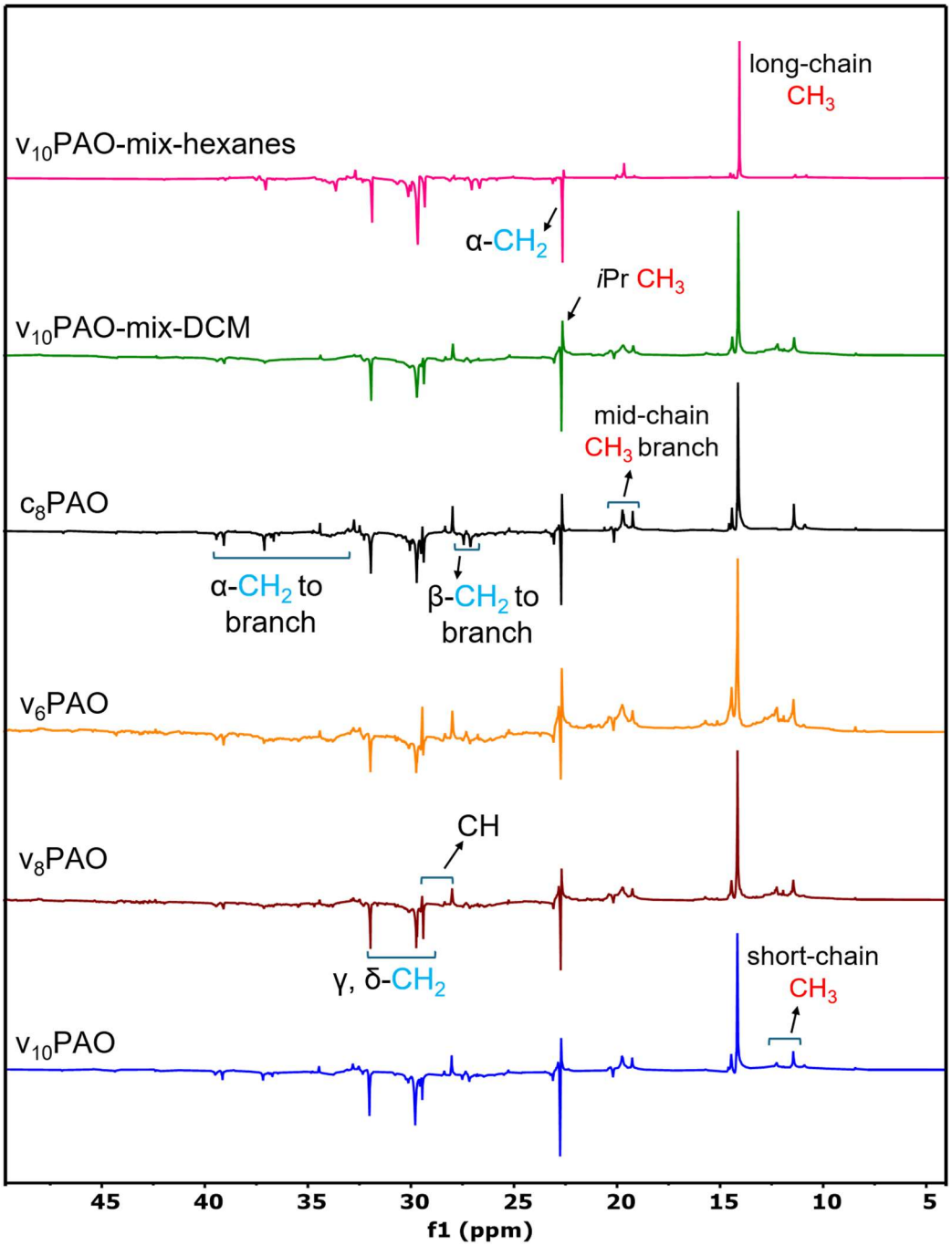

Figure S32. **DEPT 135 NMR of upcycled PVC oils and cPAO to identify methine, methylene, and methyl signals.** Methylene and methyl peaks were assigned based on prior literature on PAO microstructure. Methine peaks were assigned to positive signals above 27.0 ppm, which is outside the typical methyl group resonance range in saturated PAO structures[24,46-48].

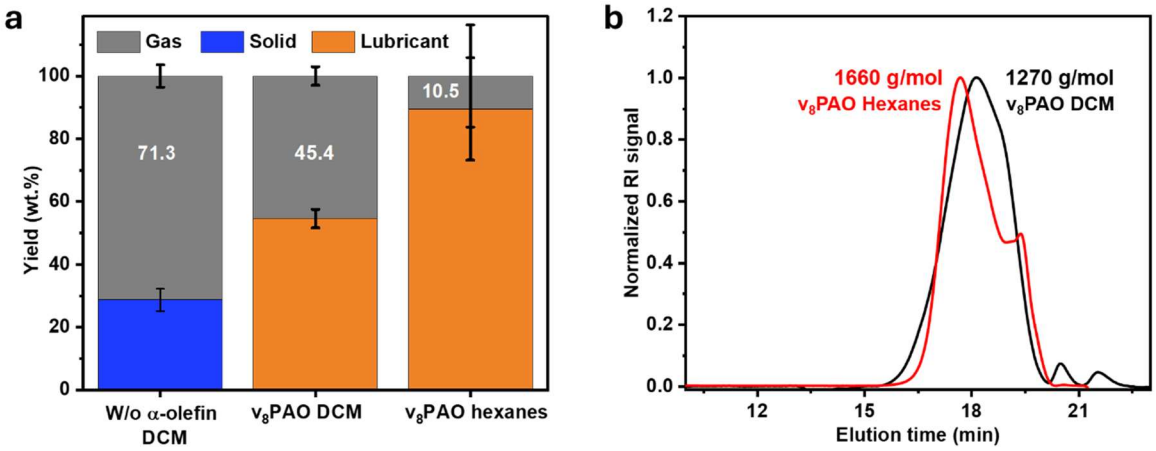

Figure S33. Effect of olefins and solvents on PVC chain degradation. a) Gas-phase yield generated without α-olefin and with α-olefins under different solvent conditions. b) SEC chromatograms of v_8PAO in DCM and hexanes, revealing a high molar mass lubricant in the isoalkane solvent.

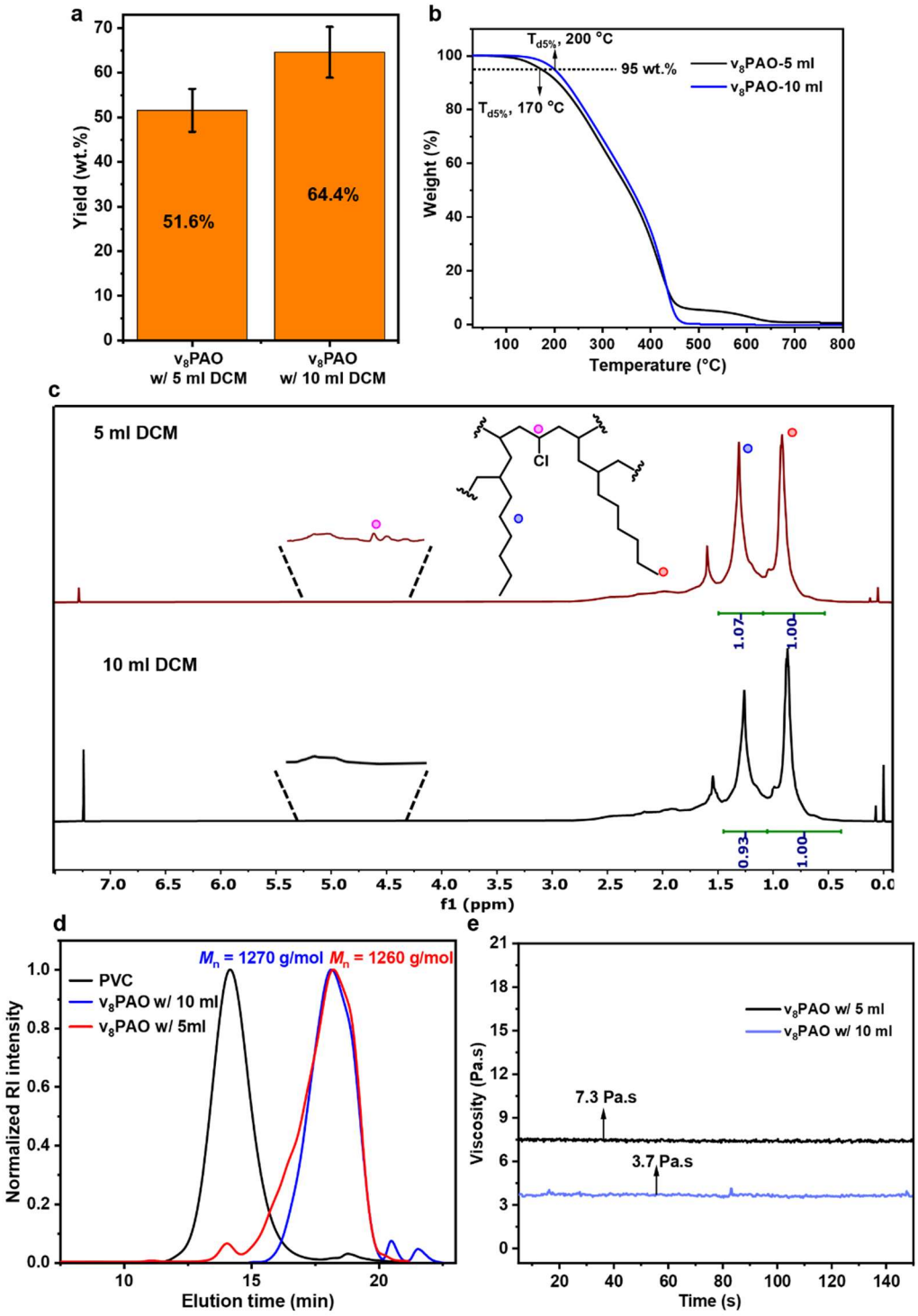

Figure S34. Effect of prolonged reaction time on $AlCl_3$ loading. a) Product yield obtained in the 48-h reaction at 25 mol% $AlCl_3$ loading vs 3 h reaction at 50 mol% $AlCl_3$ loading. b) FTIR of the products, showing residual C-Cl under low $AlCl_3$ loading conditions. c) ^1H NMR of lubricant products. Residual PVC moieties are evidenced by the triad at 4.4 ppm.

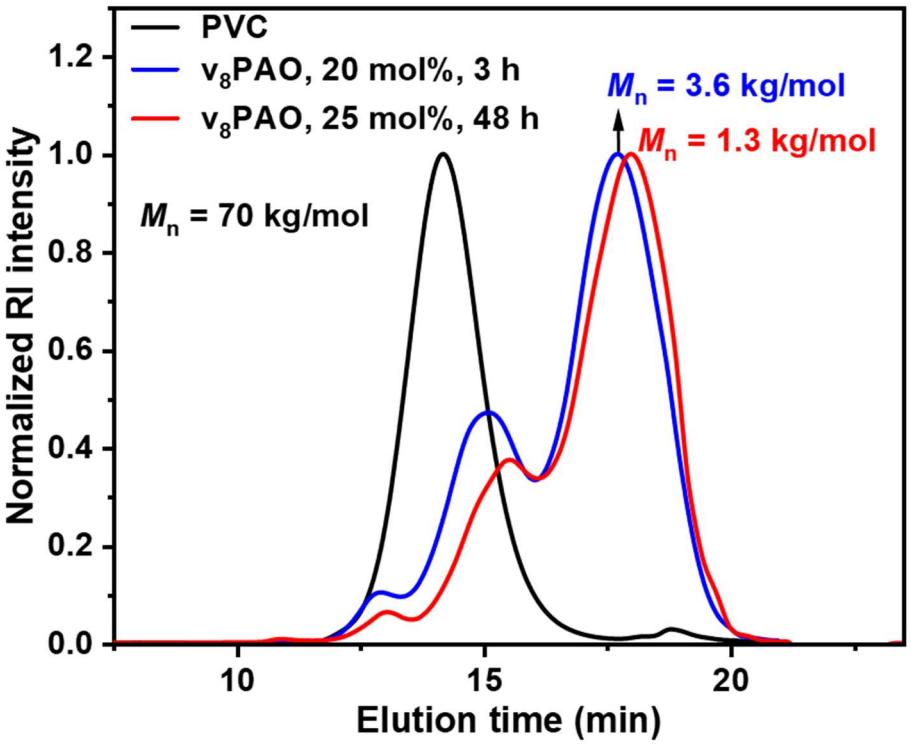

Figure S35. SEC chromatograms of the prolonged reaction under low $AlCl_3$ loading. The shoulder peaks of v_8PAO indicate high-molar-mass partially reacted and/or crosslinked PVC.

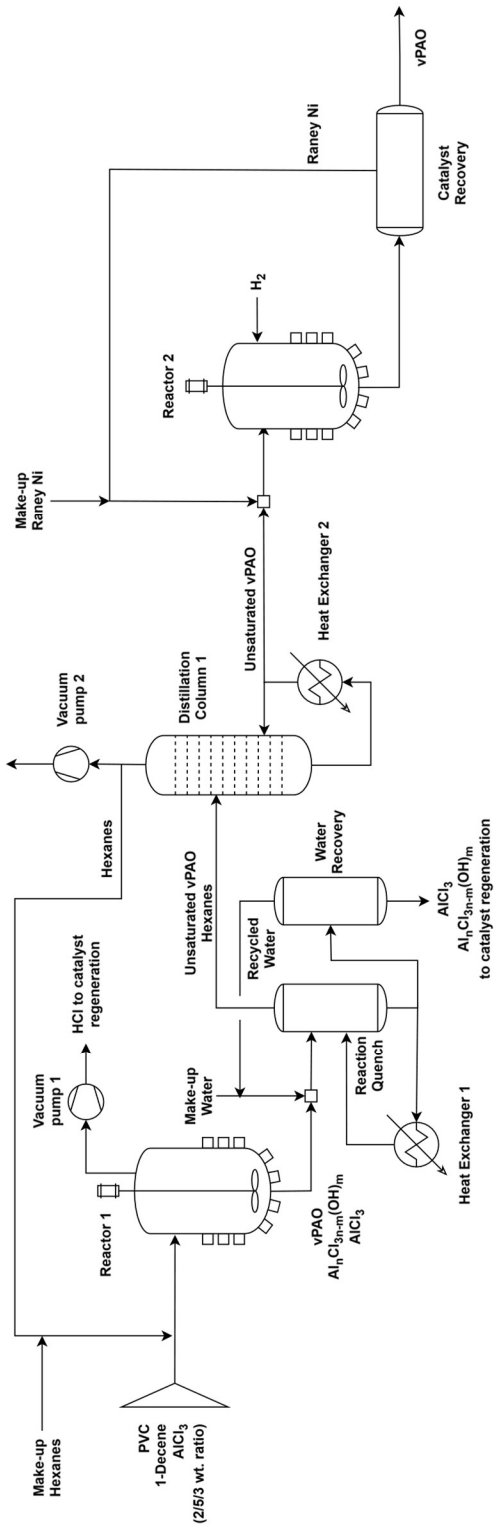

Figure S36. **A process flow diagram showing the key steps of the upcycling operation**. For simplicity, a detailed illustration of catalyst regeneration using HCl was omitted.

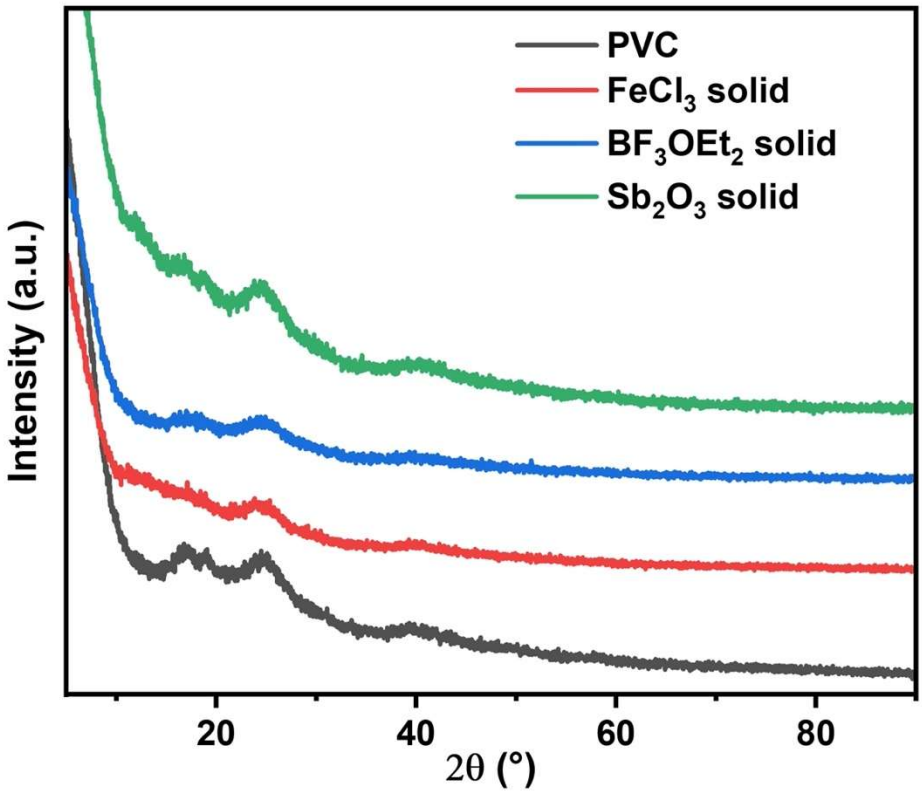

Figure S37. Powder XRD of the solid products after PVC reactions using various Lewis acids. No sharp peaks were detected. In the reaction using $FeCl_3$, the peak at $2\theta = 17$ ° diminished, suggesting partial alkylation of PVC.

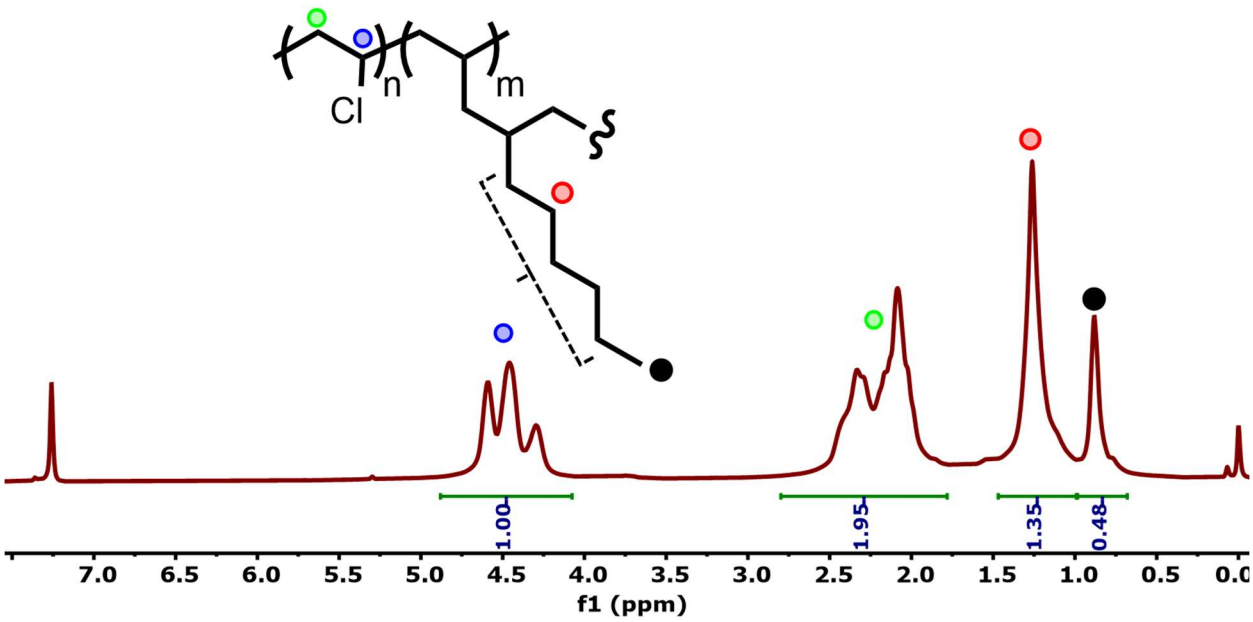

Figure S38. ^{1}H NMR of the solid product formed in the PVC upcycling reaction using $FeCl_3$ in $CDCl_3$. The presence of unreacted PVC moieties was confirmed by the triad at 4.4 ppm and the dyad at 2.2 ppm. Partial alkylation was evidenced by the alkyl chain resonance between 0.7 ppm and 1.5 ppm.

Figure S39. Solubility test of the solid product after the PVC upcycling reaction using $FeCl_3$. (left) Representative powder of the solid product. (right) A solution of the solid product (35 mg) in 1,2,4-trichlorobenzene (7 ml).

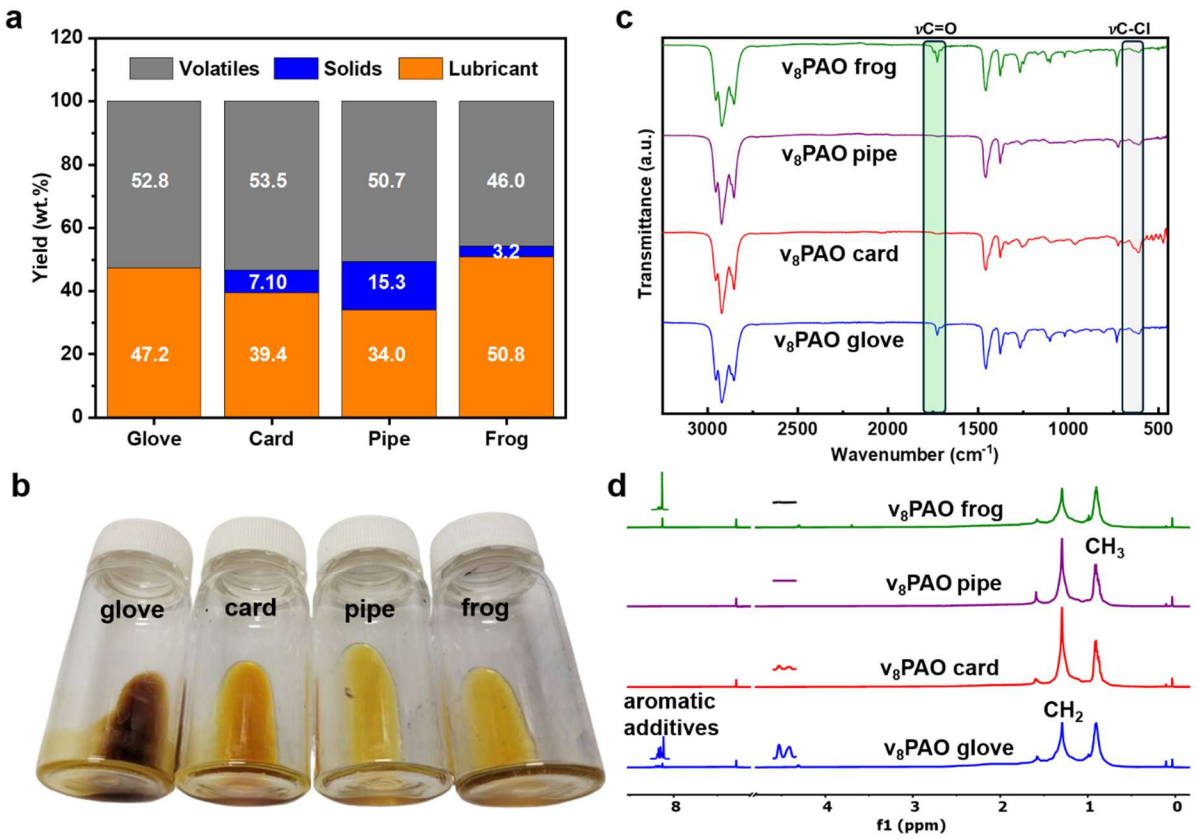

Figure S40. Upcycling of raw PVC powders with additives. a) Product yield for each type of raw PVC feedstock, without any extraction or purification processing. b) Photographs of lubricants obtained from raw PVC powders without any extraction or purification processing. c) FTIR spectra of lubricants showing both residual C-Cl from PVC and C=O from the additives. d) ^{1}H NMR spectra of the lubricants featuring methine protons in residual PVC in the card and glove-derived lubricants, as well as aromatic additives in the toy frog and glove lubricants.

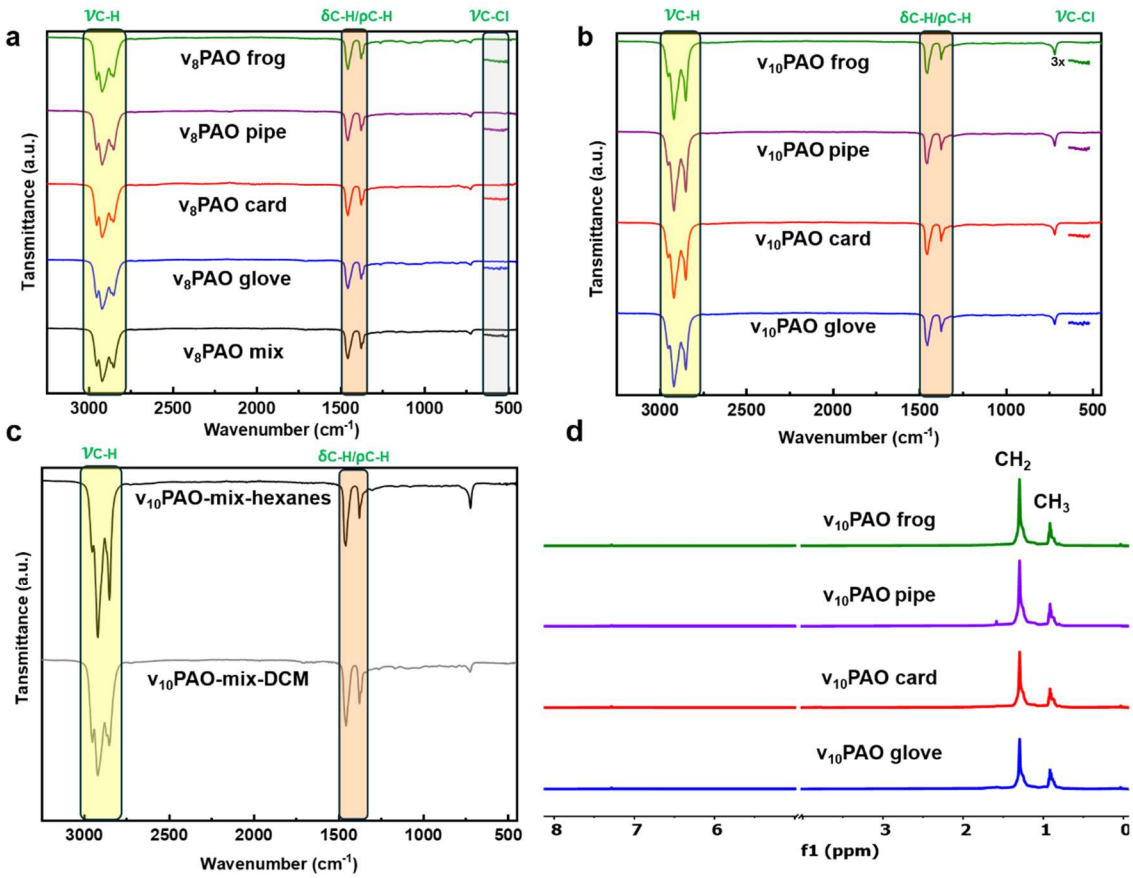

Figure S41. Structural analysis of lubricants upcycled from purified waste PVC. a) FTIR of v_8PAO synthesized from four representative PVC products (e.g., frog, pipe, card, and glove) and their mixtures. The reaction was carried out in DCM. b) FTIR of v_{10}PAO from waste PVC products and their mixtures. The reaction was carried out in hexanes. c) FTIR of v_{10}PAO from waste PVC mixtures synthesized in DCM and hexanes. d) ^{1}H NMR of v_{10}PAO synthesized from four PVC products. All spectra show complete dechlorination.

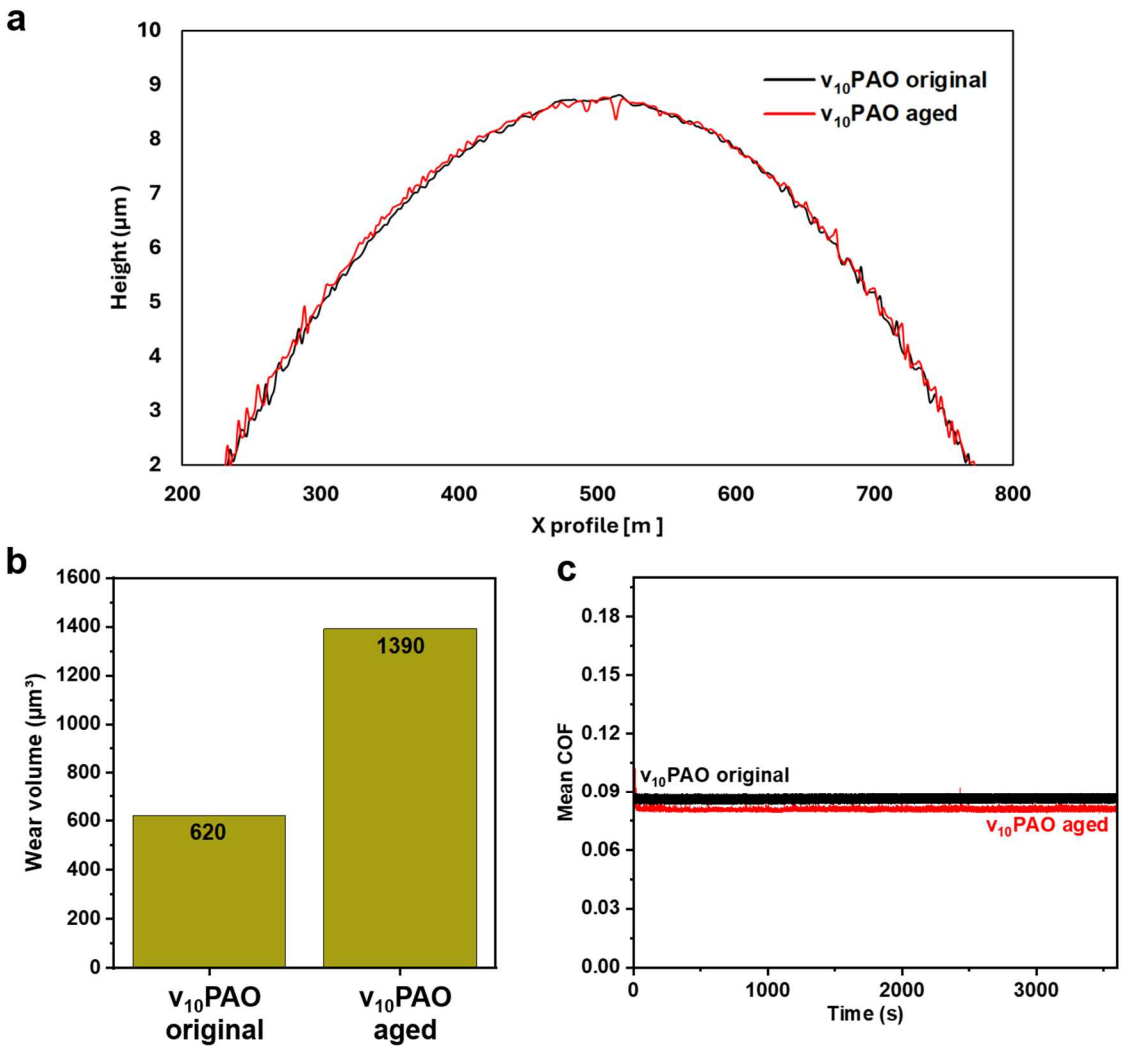

Figure S42. Effect of aging on tribological properties. a) 2D line scans over the wear scars of both the original and aged v_{10}PAO oils, showing negligible differences. b) Wear volume of original and aged v_{10}PAO oil. c) COF revealing no substantial changes between the original and aged v_{10}PAO oil.

Table S1. Effect of alpha-olefin chain length and solvent type on the branching ratio and dynamic viscosity of vPAO.

Lubricant	PVC feedstock	Solvent	I_{CH2}/I_{CH3} †	Branching Ratio (%)	Dynamic Viscosity‡ (Pa·s)
c_8PAO	lab-grade	DCM	1.23	35.5	0.10
v_{10}PAO		DCM	1.00	38.5	2.20
v_8PAO		DCM	0.93	46.0	3.70
v_6PAO		DCM	0.63	65.2	16.40
v_{10}PAO mix#	real-life waste*	DCM	0.87	38.4	2.98
		hexanes	2.65	17.1	0.37

* Waste mixture consisted of PVC cards, gloves, pipes, and toy frogs.
# v_{10}PAO mix was synthesized using 60 mol% and 50 mol% of $AlCl_3$ loading in DCM and hexanes, respectively, affording Cl-free lubricants.
† The ratio of the CH_2 and CH_3 signal integration in ^{1}H NMR.
‡ Dynamic viscosities were recorded at ~20 °C.

Table S2. Effect of $AlCl_3$ loading on I_{CH2}/I_{CH3} and dynamic viscosity of v_8PAO. The I_{CH2}/I_{CH3} ratio is indicative of the degree of branching in vPAO.

Lubricant	$AlCl_3$ loading	I_{CH2}/I_{CH3}	Molar mass, M_n (g/mol)	Dynamic Viscosity (Pa·s)
120%-v_8PAO	120 mol%	0.46	630	0.25
100%-v_8PAO	100 mol%	0.57	750	0.51
80%-v_8PAO	80 mol%	0.61	1070	1.05
60%-v_8PAO	60 mol%	0.80	1130	2.03
50%-v_8PAO	50 mol%	0.93	1270	3.70
40%-v_8PAO	40 mol%	1.09	1430	14.54

Note that all vPAO synthesized with < 40 mol% $AlCl_3$ loading yielded grease-like products, which did not flow and were not testable using a rheometer to determine the dynamic viscosity.

Table S3. Results of ion chromatography analysis. All oils contained < 100 ppm chlorine regardless of the PVC source and reaction solvent.

Sample	Compound	Peak area	Peak height	Concentration (ppm)
v_8PAO	Cl^-	2.34×10^5	1.64×10^4	<100
v_{10}PAO-mix-DCM		2.27×10^5	1.58×10^4	<100
v_{10}PAO-mix-hexanes		2.08×10^5	1.29×10^4	<100

Table S4. Effect of solvent on I_{CH2}/I_{CH3} of v_8PAO. All vPAO was synthesized at 50 mol% $AlCl_3$ loading.

sample	Solvent	I_{CH2}/I_{CH3}
v_8PAO	CH_2Cl_2	0.93
	$CHCl_3$	1.18
	CCl_4	2.48
	hexanes	2.76
	heptanes	2.19
	toluene	1.80

Table S5. ICP-MS analysis of metals in PVC powders and upcycled lubricants.

	[Ca] (ppm)	[Mg] (ppm)	[Al] (ppm)	[Ti] (ppm)	[Cr] (ppm)	[Sn] (ppm)	[Fe] (ppm)	[Zn] (ppm)
Waste PVC	15958	299	227	259	0	94	0	117
Washed PVC	2232	0	0	101	0	61	0	68
Virgin PVC	0	0	0	5	0	0	0	0
v_8PAO	0	0	0	6	0	0	0	0
v_{10}PAO-mix-hexanes	0	0	0	7	0	0	0	0

Table S6. Thermal properties of vPAO synthesized using lab-grade PVC and PVC waste

Sample	PVC feedstock	Solvent	$T_{d\ 5\%}$ (°C)	$T_{d\ 50\%}$ (°C)	T_g (°C)
c_6PAO	None	DCM	170	295	-53
c_8PAO			178	323	-62
c_{10}PAO			166	340	-77
v_6PAO	Lab-grade	DCM	176	325	-47
v_8PAO			200	362	-54
v_{10}PAO			189	364	-61
v_8PAO	Cards	DCM	187	335	-54
v_8PAO	Gloves		205	364	-53
v_8PAO	Pipes		205	367	-53
v_8PAO	Toy frogs		193	359	-50
v_{10}PAO	Mix waste*		152	323	-49
c_{10}PAO	None	Hexanes	276	420	-82
v_{10}PAO	Card	Hexanes	192	413	-76
v_{10}PAO	Glove		221	415	-83
v_{10}PAO	Pipe		261	411	-75
v_{10}PAO	Toy frog		202	424	-78
v_{10}PAO	Mix waste*		207	416	-76

* Mix waste consisted of 25 wt.% of PVC cards, 25 wt.% PVC gloves, 25 wt.% PVC pipes, and 25 wt.% PVC toy frogs.

Table S7. Key assumptions of capital investment

Fixed capital investments		
(1) Direct cost (specified as % of equipment cost)		
	Equipment	
	Other direct costs (specified as % of equipment cost)	
	Installation	40%
	Piping	66%
	Instrumentation and control	20%
	Building & Structure	20%
	Yard improvement	10%
	Service facilities	50%
	Land	6%
(2) Indirect cost (specified as % of direct cost)		
	Engineering & supervision	15%
	Legal expenses	2%
	Construction expenses	15%
(3) Others (specified as % of the direct and indirect cost)		
	Contractor's fee	5%
	Contingency	10%
Working capital: 15% of fixed capital investment		

Table S8. Other key assumptions and the prices of input and output

Assumptions	
Project length	20 years
Salvage value	0%
Depreciation method	Straight-line depreciation, under which equipment is depreciated at a constant annual rate of 1/*n*, where *n* is the depreciation period in years
Loading of 1-decene	The optimal loading of 1-decene was assumed to be 1.05 equivalents to chlorine in PVC after optimizing the olefin feed rate
Depreciation period	10 years
Annual interest rate	3%
Fixed costs, raw material and product prices	remain constant over time
PAO lubricant	$3,212/ton
PVC	$100/ton
1-Decene	$926/ton
$AlCl_3$	$329/ton
Dichloromethane	$348/ton
Nitrogen	$250/ton
Hydrogen	$1,280/ton
Raney Nickel	$16,680/ton
Operating labor	15% of the total product cost
Operating supervision	10% of the operating labor
Utilities	15% of the total product cost
Maintenance and repairs	5% of the fixed capital investment
Operating supplies	15% of maintenance and repair costs
Laboratory charges	15% of operating labor
Royalties	3% of the total product cost
Plant overhead costs	5% of the total product cost
General expenses	10% of the total product cost

Table S9. Key equipment cost evaluations

	amount	Price of each	Total price
Reactor 1	1	150,000	150,000
Reactor 2	1	100,000	100,000
Distiller	1	400,000	400,000
Pump	2	20,000	40,000
Heat exchanger	2	25,000	50,000
Others*			222,000
Total cost($)			962,000

*The costs of other auxiliaries were estimated based on 30% of the total equipment cost.

14. References

1 Beveridge, J. M., Chenot, H. M., Crich, A., Jacob, A. & Finn, M. G. Covalent Functionalization of Flexible Polyvinyl Chloride Tubing. *Langmuir* **34**, 10407-10412 (2018). https://doi.org/10.1021/acs.langmuir.7b03115

2 Assefa, M. K. & Fieser, M. E. Divergent silylium catalysis enables facile poly(vinyl chloride) upcycling to poly(ethylene-co-styrene) derivatives. *Journal of Materials Chemistry A* **11**, 2128-2132 (2023). https://doi.org/10.1039/D2TA08142C

3 Arslan, R., Atilla Tasdelen, M. & Arslan, M. Covalent modification of poly(vinyl chloride) via organometallic Barbier reaction. *Eur. Polym. J.* **177**, 111475 (2022). https://doi.org/https://doi.org/10.1016/j.eurpolymj.2022.111475

4 Wood, Z. A., Castro, E. C., Nguyen, A. N. & Fieser, M. E. Conversion of waste poly(vinyl chloride) to branched polyethylene mediated by silylium ions. *Chemical Science* **15**, 8766-8774 (2024). https://doi.org/10.1039/D4SC00130C

5 Jha, R. K., Neyhouse, B. J., Young, M. S., Fagnani, D. E. & McNeil, A. J. Revisiting poly(vinyl chloride) reactivity in the context of chemical recycling. *Chemical Science* **15**, 5802-5813 (2024). https://doi.org/10.1039/D3SC06758K

6 Moulay, S. Chemical modification of poly(vinyl chloride)—Still on the run. *Prog. Polym. Sci.* **35**, 303-331 (2010). https://doi.org/https://doi.org/10.1016/j.progpolymsci.2009.12.001

7 Starnes, W. H. Structural and mechanistic aspects of the thermal degradation of poly(vinyl chloride). *Prog. Polym. Sci.* **27**, 2133-2170 (2002). https://doi.org/https://doi.org/10.1016/S0079-6700(02)00063-1

8 Starnes, W. H. Structural Defects in Poly(vinyl chloride) and the Mechanism of Vinyl Chloride Polymerization: Comments on Recent Studies. *Procedia Chem.* **4**, 1-10 (2012). https://doi.org/https://doi.org/10.1016/j.proche.2012.06.001

9 Xu, S. *et al.* Upcycling chlorinated waste plastics. *Nat. Rev. Methods Primers* **3**, 44 (2023). https://doi.org/10.1038/s43586-023-00227-w

10 Wang, M.-M., Zhang, C.-C. & Zhang, F.-S. Recycling of spent lithium-ion battery with polyvinyl chloride by mechanochemical process. *Waste Management* **67**, 232-239 (2017). https://doi.org/https://doi.org/10.1016/j.wasman.2017.05.013

11 Kaminsky, W. Chemical recycling of plastics by fluidized bed pyrolysis. *Fuel Communications* **8**, 100023 (2021). https://doi.org/https://doi.org/10.1016/j.jfueco.2021.100023

12 Kots, P. A., Vance, B. C., Quinn, C. M., Wang, C. & Vlachos, D. G. A two-stage strategy for upcycling chlorine-contaminated plastic waste. *Nature Sustainability* **6**, 1258-1267 (2023). https://doi.org/10.1038/s41893-023-01147-z

13 Moore, J. D., Cui, S. T., Cochran, H. D. & Cummings, P. T. Rheology of lubricant basestocks: A molecular dynamics study of C30 isomers. *The Journal of Chemical Physics* **113**, 8833-8840 (2000). https://doi.org/10.1063/1.1318768

14 Nifant'ev, I. E. *et al.* Structurally uniform 1-hexene, 1-octene, and 1-decene oligomers: Zirconocene/MAO-catalyzed preparation, characterization, and prospects of their use as low-viscosity low-temperature oil base stocks. *"Appl. Catal., A"* **549**, 40-50 (2018). https://doi.org/https://doi.org/10.1016/j.apcata.2017.09.016

15 Kobayashi, M., Saitoh, M., Ishida, K. & Yachi, H. Viscosity Properties and Molecular Structure of Lube Base Oil Prepared from Fischer-Tropsch Waxes. *J. Jpn. Pet. Inst.* **48**, 365-372 (2005). https://doi.org/10.1627/jpi.48.365

16 Shao, H. *et al.* Preparation of Lubricant Base Stocks with High Viscosity Index through 1-Decene Oligomerization Catalyzed by Alkylaluminum Chloride Promoted by Metal Chloride. *Energy & Fuels* **34**, 2214-2220 (2020). https://doi.org/10.1021/acs.energyfuels.9b04104

17 Lahtela, M., Pakkanen, T. A. & Nissfolk, F. Molecular Modeling of Poly-.alpha.-olefin Synthetic Oils. *The Journal of Physical Chemistry* **99**, 10267-10271 (1995). https://doi.org/10.1021/j100025a030

18 Tran, V. H., Guyot, A., Nguyen, T. P. & Molinié, P. Poly(vinyl chloride) dehydrochlorination via the polaron mechanism. *Polym. Degrad. Stab.* **37**, 209-216 (1992). https://doi.org/https://doi.org/10.1016/0141-3910(92)90162-X

19 Jabbarzadeh, A., Atkinson, J. D. & Tanner, R. I. The effect of branching on slip and rheological properties of lubricants in molecular dynamics simulation of Couette shear flow. *Tribol. Int.* **35**, 35-46 (2002). https://doi.org/https://doi.org/10.1016/S0301-679X(01)00089-5

20 Ji, L. *et al.* Effect of different molecular characteristics on the lubrication behavior of polysaccharide solutions. *Carbohydr. Polym.* **297**, 120000 (2022). https://doi.org/https://doi.org/10.1016/j.carbpol.2022.120000

21 Khalyavina, A., Häußler, L. & Lederer, A. Effect of the degree of branching on the glass transition temperature of polyesters. *Polymer* **53**, 1049-1053 (2012). https://doi.org/https://doi.org/10.1016/j.polymer.2012.01.020

22 Katsukawa, R., Van Sang, L., Tomiyama, E. & Washizu, H. High-Pressure Lubrication of Polyethylethylene by Molecular Dynamics Approach. *Tribol. Lett.* **70**, 101 (2022). https://doi.org/10.1007/s11249-022-01638-8

23 Van Sang, L. Simulated Tribological Properties of Pure and Mixed-Base PAO Oils. *Langmuir* **41**, 19481-19492 (2025). https://doi.org/10.1021/acs.langmuir.5c02218

24 Rahbar, A., Bahri-Laleh, N. & Nekoomanesh-Haghighi, M. Microstructural study on low viscosity poly-α-olefin oils synthesized via AlCl3/H2O cationic system in the present of xylene and heptane solvents. *Fuel* **302**, 121111 (2021). https://doi.org/https://doi.org/10.1016/j.fuel.2021.121111

25 Mashayekhi, M., Moballegh, L., Bahri-Laleh, N., Sadjadi, S. & Poater, A. Ionic liquids as modifier for the oligomerization of α-olefins to reactive poly (α-olefins) via traditional AlCl3 catalyst. *Molecular Catalysis* **547**, 113403 (2023). https://doi.org/https://doi.org/10.1016/j.mcat.2023.113403

26 Wallace, C. H. & Willard, J. E. The Exchange Reaction between Aluminum Chloride and Carbon Tetrachloride1. *Journal of the American Chemical Society* **72**, 5275-5281 (1950). https://doi.org/10.1021/ja01167a136

27 Li, Z. *et al.* Silica-supported aluminum chloride: A recyclable and reusable catalyst for one-pot three-component Mannich-type reactions. *J. Mol. Catal. A: Chem.* **272**, 132-135 (2007). https://doi.org/https://doi.org/10.1016/j.molcata.2007.03.029

28 Zhu, Y. *et al.* AlCl3·6H2O-Catalyzed Friedel-Crafts Alkylation of Indoles by the para-Quinone Methide Moiety of Celastrol. *Molecules* **22**, 742 (2017).

29 Fonseca, J. D., Grause, G., Kameda, T. & Yoshioka, T. Effects of steam on the thermal dehydrochlorination of poly(vinyl chloride) resin and flexible poly(vinyl chloride) under

atmospheric pressure. *Polym. Degrad. Stab.* **117**, 8-15 (2015). https://doi.org/https://doi.org/10.1016/j.polymdegradstab.2015.03.011

30 Boborodea, A., Mirabella, F. M. & O'Donohue, S. Characterization of Low-Density Polyethylene in Dibutoxymethane by High-Temperature Gel Permeation Chromatography with Triple Detection. *Chromatographia* **79**, 971-976 (2016). https://doi.org/10.1007/s10337-016-3047-7

31 Burn, L. S. The influence of titanium dioxide on the durability of uPVC pipe. *Polym. Degrad. Stab.* **36**, 155-167 (1992). https://doi.org/https://doi.org/10.1016/0141-3910(92)90152-U

32 Yang, T.-C., Noguchi, T., Isshiki, M. & Wu, J.-H. Effect of titanium dioxide on chemical and molecular changes in PVC sidings during QUV accelerated weathering. *Polym. Degrad. Stab.* **104**, 33-39 (2014). https://doi.org/https://doi.org/10.1016/j.polymdegradstab.2014.03.023

33 Pi, H., Guo, S. & Ning, Y. Mechanochemical improvement of the flame-retardant and mechanical properties of zinc borate and zinc borate–aluminum trihydrate-filled poly(vinyl chloride). *J. Appl. Polym. Sci.* **89**, 753-762 (2003). https://doi.org/https://doi.org/10.1002/app.12202

34 Bisley International. *What Additives Are Added to PVC*, 2022).

35 IMARC. *Polyalphaolefin (PAO) Prices, Trend, Chart, Demand, Market Analysis, News, Historical and Forecast Data Report 2025 Edition*, <https://www.imarcgroup.com/polyalphaolefin-pricing-report> (2025).

36 Statista. *Forecast production costs for hydrogen in the United States in 2030, by scenario and production type* <https://www.statista.com/statistics/1179498/us-hydrogen-production-costs-forecast/> (2025).

37 IMARC. *1-Decene Pricing Report 2024: Price Trend, Chart, Market Analysis, News, Demand, Historical and Forecast Data*, <https://www.imarcgroup.com/1-decene-pricing-report> (2024).

38 IMARC. *Aluminium Chloride Pricing Report 2024: Price Trend, Chart, Market Analysis, News, Demand, Historical and Forecast Data*, <https://www.imarcgroup.com/aluminium-chloride-pricing-report> (2023).

39 CHEMANALYST. *Nitrogen Price Trend and Forecast*, <https://www.chemanalyst.com/Pricing-data/nitrogen-1097> (2025).

40 IMARC. *Hexane Prices, Trend, Chart, Demand, Market Analysis, News, Historical and Forecast Data Report 2025 Edition*, <https://www.imarcgroup.com/hexane-pricing-report> (2025).

41 Resource, P. *Nickel Price Trend and Forecast*, <https://www.procurementresource.com/resource-center/nickel-price-trends> (2025).

42 Peters, M. & Timmerhaus, K. *Plant Design and Economics for Chemical Engineers*. 4th edn, 181-185 (McGraw-Hill, 1991).

43 Peters, M. S. & Timmerhaus, K. D. *Plant Design and Economics for Chemical Engineers*. 4th edn, 192-209 (McGraw-Hill, 1991).

44 Akhrem, I. & Orlinkov, A. Polyhalomethanes Combined with Lewis Acids in Alkane Chemistry. *Chemical Reviews* **107**, 2037-2079 (2007). https://doi.org/10.1021/cr970005n

45 Soulsby, D. Using 1H NMR Spectroscopy to Study the Free Radical Chlorination of Alkanes. *J. Chem. Educ.* **97**, 2286-2290 (2020). https://doi.org/10.1021/acs.jchemed.0c00160

46 Montanari, L., Montani, E., Corno, C. & Fattori, S. NMR molecular characterization of lubricating base oils: Correlation with their performance. *Appl. Magn. Reson.* **14**, 345-356 (1998). https://doi.org/10.1007/BF03161900

47 Verdier, S., Coutinho, J. A. P., Silva, A. M. S., Alkilde, O. F. & Hansen, J. A. A critical approach to viscosity index. *Fuel* **88**, 2199-2206 (2009). https://doi.org/https://doi.org/10.1016/j.fuel.2009.05.016

48 Dong, S. Q., Mi, P. K., Xu, S., Zhang, J. & Zhao, R. D. Preparation and Characterization of Single-Component Poly-α-olefin Oil Base Stocks. *Energy & Fuels* **33**, 9796-9804 (2019). https://doi.org/10.1021/acs.energyfuels.9b02938